

Non-negatively constrained least squares and parameter choice by the residual periodogram for the inversion of electrochemical impedance spectroscopy

Jakob Hansen^a, Jarom Hogue^a, Grant Sander^a, Rosemary A Renault^{a,*}, Sudeep C Popat^b

^a*School of Mathematical and Statistical Sciences, Arizona State University, Tempe, AZ 85287-1804, USA*

^b*Swette Center for Environmental Biotechnology, Biodesign Institute, Arizona State University, Tempe, AZ 85287, USA*

Abstract

The inverse problem associated with electrochemical impedance spectroscopy requiring the solution of a Fredholm integral equation of the first kind is considered. If the underlying physical model is not clearly determined, the inverse problem needs to be solved using a regularized linear least squares problem that is obtained from the discretization of the integral equation. For this system, it is shown that the model error can be made negligible by a change of variables and by extending the effective range of quadrature. This change of variables serves as a right preconditioner that significantly improves the condition of the system. Still, to obtain feasible solutions the additional constraint of non-negativity is required. Simulations with artificial, but realistic, data demonstrate that the use of non-negatively constrained least squares with a smoothing norm provides higher quality solutions than those obtained without the non-negative constraint. Using higher-order smoothing norms also reduces the error in the solutions. The L-curve and residual periodogram parameter choice criteria, which are used for parameter choice with regularized linear least squares, are successfully adapted to be used for the non-negatively constrained Tikhonov least squares problem. Although these results have been verified within the context of the analysis of electrochemical impedance spectroscopy, there is no reason to suppose that they would not be relevant within the broader framework of solving Fredholm integral equations for other applications.

Keywords: Inverse problem, non-negative least squares, regularization, ill-posed, residual periodogram

2000 MSC: 65F10, 45B05, 65R32

*Corresponding Author: Rosemary Renault, 480 965 3795

Email addresses: jkhans2@asu.edu (Jakob Hansen), jdhogue@asu.edu (Jarom Hogue), gksander@asu.edu (Grant Sander), renaut@asu.edu (Rosemary A Renault), scp@asu.edu (Sudeep C Popat)

URL: math.asu.edu/~rosie (Rosemary A Renault)

1. Introduction

We consider the numerical solution of ill-posed inverse problems that are motivated by measurements of electrochemical impedance spectra from which a model of the underlying physical reaction mechanisms is desired. There is extensive literature on a wide range of applications in which the same, or similar models can be applied. These include measurements for solid oxide fuel cells [5, 19, 20, 21, 22, 24, 30, 32], microbial fuel cells [27], as well as of physiological parameters, and from a diverse range of dielectric models, [2, 23, 26, 34]. In these applications the unknown distribution function of relaxation times (DRT) is related to a set of impedance measurements by the Fredholm integral equation

$$Z(\omega) = R_0 + R_{\text{pol}} \int_0^\infty \frac{g(t)}{1 + i\omega t} dt, \quad (1.1)$$

where ω is angular frequency, t is time, and $g(t)$ is the desired DRT with normalization $\int_0^\infty g(t) dt = 1$.

There are several models used to represent the individual processes of a DRT, many of which are mostly used for the analysis of dielectric materials and are described in [2]. Several are directly applicable to the fuel cell modeling case, where they usually take the form of theoretical circuit components used in constructing equivalent circuit models. Equivalent circuit elements used for fuel cell modeling include the Cole-Cole (also known as RQ or ZARC) element, the Generalized Finite-Length Warburg element, and the Gerischer impedance [2, 18, 24]. In analysis of specific fuel cell designs a log-normal form for the DRT has also been used [26, 27]. Here we focus our investigations on the Cole-Cole DRT, which can be rendered temperature independent only in the limiting cases of $\beta \rightarrow 0, 1$, and the temperature independent lognormal DRT, denoted throughout by RQ and LN, respectively.

The RQ impedance is a generalization of a simple parallel RC circuit and for a single process has an impedance given by

$$Z_{\text{RQ}}(\omega) = \frac{1}{1 + (i\omega t_0)^\beta}, \quad (1.2)$$

where t_0 is the point of maximum distribution, and β is a shape parameter controlling the width of the distribution. The corresponding DRT is

$$g_{\text{RQ}}(t) = \frac{1}{2\pi t} \frac{\sin \beta\pi}{\cosh\left(\beta \ln\left(\frac{t}{t_0}\right)\right) + \cos \beta\pi}, \quad (1.3)$$

which reduces to the Dirac delta distribution when $\beta = 1$, [2]. There is, however, no analytic form for the impedance corresponding to the log-normal DRT given by

$$g_{\text{LN}}(t) = \frac{1}{t\sigma\sqrt{2\pi}} \exp\left(-\frac{(\ln(t) - \mu)^2}{2\sigma^2}\right). \quad (1.4)$$

Although a number of options have been presented in the literature for geometrically assessing the parameterization of the DRT from impedance data for a single physical process, e.g. as noted in [34], for given measured and noisy impedance data from multiple processes

there are effectively only two basic approaches that may be considered to estimate the DRT. When a specific analytic but parameter dependent form for the impedance is known, as in (1.2), parametric nonlinear least squares (NLS) fitting may be used to determine the underlying parameters of the impedance and hence of the DRT, [23]. On the other hand, when no analytic representation of the impedance is available, as in (1.4), it is still possible, but more computationally expensive, to apply a parametric nonlinear fit by using direct numerical integration of (1.1). In either case, an alternative is to apply a linear least squares (LLS) fit directly to the DRT, but this is also challenging due to the general ill-posedness of the problem, e.g. [4, 11, 13, 14, 33]. Both approaches, as well as the geometric analyses, have been extensively considered in the literature, e.g. [2]. When the model for the DRT is not known, perhaps when the physical process is not completely understood or the number of processes has not been determined, the only option is to fit directly to the DRT, without identifying its specific parameterization.

Before further pursuing the LLS fit, we illustrate in Section 2 the use of direct NLS fitting for a simple one-process example in order to emphasize the (self-evident) significance of the prior knowledge of the model. Assuming the wrong model leads to apparently robust data fitting, while at the same time potentially leading to incorrect conclusions about the DRT parameterization. With this conclusion we move in Section 3 to an analysis of the system describing the LLS fitting that arises when approximating (1.1) discretely. The direct discretization of (1.1) leads to two ill-conditioned systems of equations, for the real and imaginary parts separately. Most literature on the problem suggests the use of LLS for the systems obtained in this way, in conjunction with regularization to stabilize the estimation of the solution, [19, 35]. In contrast, it was suggested in [24], that rather than estimating the DRT in the given t -space, a transformation to s -space via $s = \log(t)$ would be preferable and that the resulting ill-posed system be solved using a non-negative least squares (NNLS) algorithm, specifically imposing the constraint that the DRT is a positive distribution. In Section 3.2 we investigate the modeling error that arises when using the s -space transformation, leading to new results that quantify the total modeling error due to discretization and truncation in (1.1) for both real and imaginary terms. The results go beyond those presented in [27] for the t -space formulation, by providing error estimates which are primarily determined by the kernel $h(\omega, t) = (1 + i\omega t)^{-1}$, only relying on standard smoothness and decay conditions for the DRT functions.

The numerical algorithms for the estimation of the DRT are discussed in Section 4. First it is demonstrated that the s -transformation serves as a **right preconditioner**, leading to more stable estimation of the underlying basis for the solution when the time discretization is chosen appropriately in relation to the frequency measurements. Still the model remains ill-conditioned, and solution techniques using regularization are required, introducing the need for determination of a regularization parameter that weights the regularization term. Estimation of this regularization parameter for Tikhonov regularization is well-studied in the literature e.g. [11, 33]. We therefore give just a brief and standard overview of regularized LLS in Section 4.3. On the other hand, the estimation of the regularization parameter in the context of non-negatively (NN) constrained Tikhonov regularization is less well-studied. Thus to put the new work in context we focus on the estimation of the regularization parameter using the L-curve (LC) and residual periodogram (RP), or its normalized cumulative periodogram (NCP). This discussion leads to new regularization parameter estimation tech-

niques for the NN-constrained Tikhonov LS problem. In particular, the LC and NCP parameter estimation techniques are extended to the NNLS algorithm, with minimal additional algorithmic development, Section 4.4.

Finally, the theoretical developments are verified and evaluated for a set of impedance datasets, consisting of two and three physical processes, which are motivated by examples that are seen from practical configurations. The presented results justify both the use of inclusion of the non-negativity constraint for finding approximate DRTs from multiple physical processes, and the use of the NCP and LC for estimating the regularization parameter within this context. To verify that our approach is sufficiently general, numerical simulations use two different algorithms for the solution of the NNLS problem, namely the Matlab function `lsqnonneg` which is based on the algorithm in [17], and the CVX software package, [8, 9]. Our results verify that indeed the LC and NCP techniques can be used for optimal regularization parameter determination when solving the NN-constrained Tikhonov least squares problem. The latter is of more general use for ill-posed systems of linear equations with NN-constraints. Conclusions of the work are provided in Section 6.

2. Parametric NLS Fitting: Distinguishing between models for one process

We investigate parametric nonlinear fitting to impedance data given by (1.1) with $R_0 = 0$ and $R_{\text{pol}} = 1$ (without any loss of generality). For a given DRT, simulated data for $Z = Z_1 - iZ_2$ were generated for realistic frequencies $\omega \in [10^{-2}, 10^5]$ sampled logarithmically at 65 points, providing the *exact* fitting vector $[Z_1; Z_2]$ of length 130. The exact data were generated for the RQ and LN DRTs, (1.3) and (1.4), respectively, with parameters $t_0 = 0.1$, $\beta = 0.7203$ and $\sigma = \ln(2.3)$ chosen to provide DRTs aligned with respect to the location and height of the peak in the $s = \ln(t/t_0)$ space, see Figure 1(b), $\beta = (2/\pi) \arctan((\sqrt{2\pi}/\sigma) \exp(-\sigma^2/2))$, see Section 3.1 and [10]. For the RQ impedance (1.2) was used to provide the vector Z , whilst for the LN impedance the data were generated by Matlab's `integrate()` function with the bounds 0 and `Inf`. The resulting Nyquist plots (complex plot of Z) and components Z_1 and Z_2 are quite similar, see Figures 1(c)-1(e), and identification of the underlying model from such data, particularly when contaminated by noise, may not be possible.

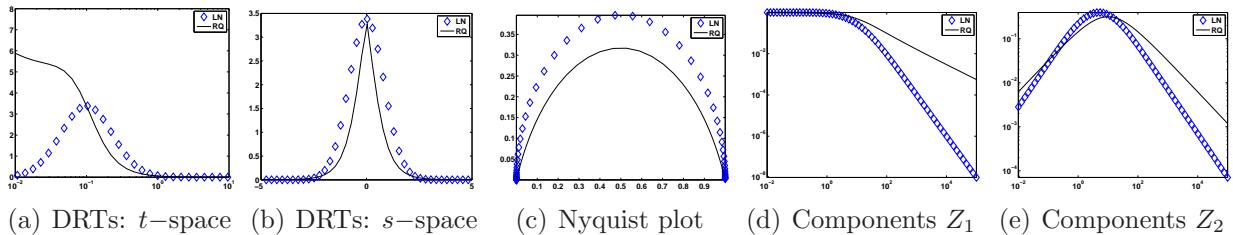


Figure 1: Simulated *exact* data measured at 65 logarithmically spaced points in ω . In each case the solid line indicates the RQ functions and the \diamond symbols the LN functions.

To simulate noisy measurements, white noise at a level η_j was added according to

$$\hat{Z}_{ij} = Z + \eta_j \mathbf{e}_i, \quad (2.1)$$

where \hat{Z}_{ij} denotes the noisy data, and the vector \mathbf{e}_i is the i^{th} column of the array of size 130×50 generated using the Matlab function `randn`, corresponding to 50 realizations of white noise, for noise levels η_j $j = 1 : 21$ logarithmically spaced between 10^{-6} and $10^{-2.5}$. The choice of the highest noise level used here was determined by comparing the obtained values for \hat{Z} as compared to data seen in practice. The lowest noise level corresponds to effectively noise-free data, but avoids the *inverse crime* by assuring that the data used in the inversion were not exactly prescribed by the underlying forward model. Nonlinear fitting was performed using the Matlab function `lsqcurvefit()` initialized with $\beta = 0.8$, $\sigma = \ln(2)$, and $t_0 = 1/\omega_0$, where ω_0 is obtained as the argument of the dominant peak value in Z_2 , as is commonly used to find the value t_0 [2]. Bounds $0 < t_0 < 100$, and $0.1 < \beta, \sigma < 1$ were imposed. Further, scaling of each DRT was introduced through a parameter α satisfying $0 < \alpha < 1.1$ initialized with $\alpha = 1$.

Two fittings were performed for each Z_{ij} , one assuming the *correct* DRT and one assuming the *incorrect* DRT, i.e. given Z generated for the RQ DRT a fit was performed assuming the *correct* RQ impedance and the *incorrect* LN impedance values. Similarly for the LN impedance values, *correct* fitting was performed by fitting with a LN DRT, and *incorrect* fitting by an RQ DRT. When using the RQ DRT for fitting the analytic form of the impedance was used, whilst for the LN DRT all calculations used the Matlab `integrate()` function. Hence for each noise level and realization four fitting pairs were considered, RQ to RQ, LN to RQ, LN to LN, and RQ to LN. For fixed noise level η_j and each fitting pair the mean and variance of the residual calculated over the 50 realizations was calculated. Figure 2 demonstrates the imperfect residuals over all noise levels for the *mismatched* fitting, and the increasing, but relatively smaller, residuals for the *matched* fittings. Further, fitting to the LN by RQ yields a smaller residual than fitting RQ by LN. In Figure 2 the 95% confidence bounds determined by the variance of the residual are very tight, indicating the robustness of the process.

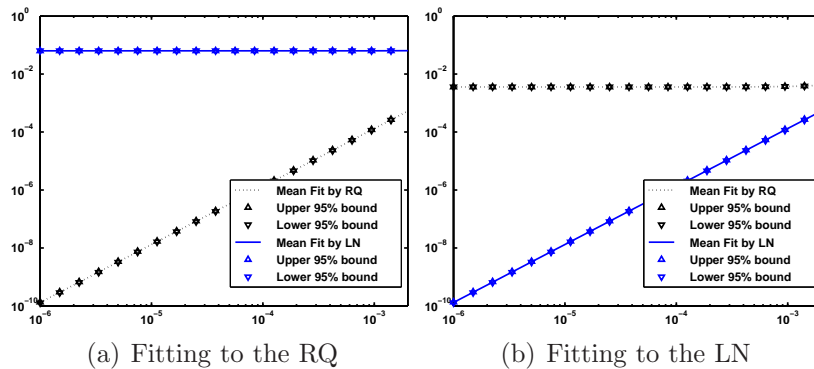


Figure 2: Residual norms fitting one process to the impedance spectrum of a DRT consisting of one process with white noise in subfigure 2(a) the RQ process and in subfigure 2(b) the LN process.

To obtain a clearer picture of the quality of the fit, the mean and standard deviation in the estimates for the underlying parameters for three different noise levels are given in Tables 1-2. In each case the *matched* fitting does a good job of parameter estimation for all noise levels, while the *mismatched* fitting is consistently wrong. Fitting the RQ impedance with the assumption of a LN DRT generates data that suggests the peak position has moved

to the left, and the peak is relatively higher, Figure 3(a). Fitting the LN impedance by a RQ DRT generates a fit moved to the right with the height quite well-preserved, Figure 3(b). However, the processes are still aligned in the $s = \log(t/t_0)$ space, Figures 3(c)-3(d), each plotted with respect to the identified t_0 .

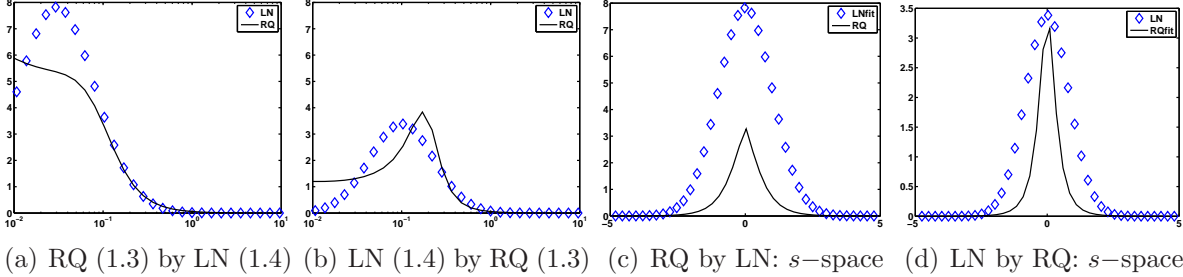


Figure 3: Fitting functions with the consistent mean values obtained and reported in Tables 1-2. In Figures 3(a) and 3(c) fitting the RQ with the LN, and in Figures 3(b)-3(d) fitting the LN with the RQ.

We conclude that if the information on the underlying DRT is not known, fitting based on the parameters of the DRT itself will lead to misleading interpretation of the results. Consequently, LLS fitting which simply finds an estimate for the DRT, without finding its parameterization, is the only feasible option for understanding the physical processes when the precise model has not been determined. We also observe that the fitting as seen in the s -space is much more informative in detecting differences and similarities of the DRTs. Of course these results are for the case of a single process. In practice multiple processes are generally exhibited and the impedance fitting is then also less robust in separating the linear combinations, even when the model is predetermined.

Fit	Parameter	True	Noise level η		
			$1e-6$	$5.6e-5$	$3.2e-3$
RQ to RQ	β	0.72	0.72($5e-07$)	0.72($3e-05$)	0.72($1e-03$)
RQ to RQ	t_0	0.10	0.10($1e-07$)	0.10($6e-06$)	0.10($4e-04$)
RQ to RQ	α	1.00	1.00($3e-07$)	1.00($1e-05$)	1.00($8e-04$)
LN to RQ	σ	0.83	1.00($8e-16$)	1.00($3e-14$)	1.00($5e-09$)
LN to RQ	t_0	0.10	0.03($4e-08$)	0.03($2e-06$)	0.03($1e-04$)
LN to RQ	α	1.00	0.97($2e-07$)	0.97($1e-05$)	0.97($7e-04$)

Table 1: Mean and standard deviation of absolute errors for obtained parameters for fitting to the RQ DRT.

Fit	Parameter	True	Noise level η		
			$1e-6$	$5.6e-5$	$3.2e-3$
RQ to LN	β	0.72	$0.86(4e-07)$	$0.86(2e-05)$	$0.86(1e-03)$
RQ to LN	t_0	0.10	$0.20(2e-07)$	$0.20(1e-05)$	$0.20(6e-04)$
RQ to LN	α	1.00	$1.01(3e-07)$	$1.01(1e-05)$	$1.01(8e-04)$
LN to LN	σ	0.83	$0.83(2e-06)$	$0.83(1e-04)$	$0.83(5e-03)$
LN to LN	t_0	0.10	$0.10(3e-07)$	$0.10(2e-05)$	$0.10(9e-04)$
LN to LN	α	1.00	$1.00(2e-07)$	$1.00(1e-05)$	$1.00(8e-04)$

Table 2: Mean and standard deviation of absolute errors for obtained parameters for fitting to the LN DRT.

3. Nonparametric Linear Least-Squares

3.1. Numerical Quadrature

When a model for the physical system has not been established, a nonparametric method of estimating its DRT must be used. The most straightforward method of discretization, discussed at length in [27] with respect to the introduced model error, uses the trapezoidal rule for quadrature with logarithmically spaced points in time to generate matrices A_1 and A_2 approximating the real and imaginary integral operators $h(\omega, t) = h_1(\omega, t) - ih_2(\omega, t)$ in (1.1). In [24] it was suggested to use a change of variables for the integration before obtaining the quadrature formulae but no discussion or analysis of the potential advantages or disadvantages was provided. Let $s = \ln t$, then

$$Z(\omega) = \int_0^\infty h(\omega, t)g(t) dt = \int_{-\infty}^\infty h(\omega, e^s)f(s) ds, \quad f(s) := tg(t). \quad (3.1)$$

For the DRTs (1.3)-(1.4) we obtain the functions

$$f_{\text{RQ}}(s) = \frac{1}{2\pi} \frac{\sin(\beta\pi)}{(\cosh(\beta(s - \ln(t_0))) + \cos(\beta\pi))} \quad (3.2)$$

$$f_{\text{LN}}(s) = \frac{1}{\sigma\sqrt{2\pi}} \exp\left(-\frac{(s - \mu)^2}{2\sigma^2}\right), \quad \ln(t_0) = \mu - \sigma^2, \quad (3.3)$$

A motivation for this change of variables is to improve the interpretation of the graph of the function when plotted on the linear scale for s as compared to the logarithmic scale for t , see e.g. Figure 1(b).

In [27, (8)-(10)] formulae for the trapezoidal quadrature weights a_n in

$$\int_0^\infty h(\omega, t)g(t) dt \approx \int_{T_{\min}}^{T_{\max}} h(\omega, t)g(t) dt \approx \sum_{n=1}^N a_n h(\omega, t_n)g(t_n), \quad (3.4)$$

show that a_n are dependent on the logarithmic spacing for t , $t_{n+1} - t_n = (\Delta t)_{n+1} = t_n(10^{\Delta t} - 1)$, where Δt is constant.¹ The same rule applied for the integral with respect to the s

¹We note the error in [27] which gives these in terms of log rather than ln.

variable, chosen so that $t_n = e^{s_n}$, gives constant $\Delta s = s_{n+1} - s_n = \ln(t_{n+1}) - \ln(t_n) = \ln(10)\Delta t$. With the standard notation that the double prime on the summation indicates that first and last terms are halved, this yields, with $s_1 = s_{\min} = \ln(T_{\min})$ and $s_N = s_{\max} = \ln(T_{\max})$

$$\int_{-\infty}^{\infty} h(\omega, e^s) f(s) ds \approx \int_{s_{\min}}^{s_{\max}} h(\omega, e^s) f(s) ds \approx \Delta s \sum_{n=1}^N {}'' h(\omega, e^{s_n}) f(s_n). \quad (3.5)$$

It is of interest to further investigate the impact of this change of variables on the condition of the resulting systems of equations and on the modeling error obtained from (3.5) so as to justify the use of the s -space formulation rather than the t -space formulation. This follows the similar investigation that was presented in [27] for (3.4). The discretization requires the choice of values for T_{\min} and T_{\max} , as well as the number of points N used in the discretization of $f(s)$ or $g(t)$. Since in this problem t and ω have a reciprocal relationship, as noted in, e.g., [19, 30], we will assume the range for t is reciprocal to the given range for ω , i.e., $T_{\max} = 1/\omega_{\min}$ and $T_{\min} = 1/\omega_{\max}$. Forthwith we will use s_1 and s_N to denote s_{\min} and s_{\max} , and we reiterate that N depends on the number of samples for the impedance.

3.2. Model error

The model error involved in the discretization of the integral operators stems from two sources: the truncation of the improper integral and the approximation of the integral by a finite quadrature rule. It will be shown here that the model error can be reduced to a negligible level given reasonable assumptions on the DRT.

3.2.1. Quadrature error

Bounds for the quadrature error for the logarithmically-spaced trapezium rule (3.4) applied for the lognormal $g(t)$ (1.4) were shown in [27, (23)]. Because of the use of the variable spacing the error bound for each term of the quadrature varies with t_n , and thus a rapidly decreasing integrand as $t \rightarrow \infty$ is necessary in order to control the error. It is well-known that the quadrature error for the standard constant spacing composite trapezium rule is given by, where we use $H(s) = h(\omega, e^s) f(s)$ and $|H''(\zeta_n)| := \max_{s \in [s_n, s_{n+1}]} |H''(s)|$,

$$|E_{\text{quad}}| \leq \sum_{n=1}^{N-1} \frac{|H''(\zeta_n)| (\Delta s)^3}{12} = \frac{(\Delta s)^3}{12} \sum_{n=1}^{N-1} |H''(\zeta_n)| = \frac{(s_N - s_1)^3}{12N^2} |H''(\zeta)| \quad (3.6)$$

for some $\zeta \in [s_1, s_N] := I_s$, assuming appropriate continuity of $H(s)$ on I_s [1].

Figures 4-5 contrast the quadrature error as a function of ω using $N = 65$ for (3.4) and (3.5), the t and s integrals, respectively, for the two DRTs (1.3)-(1.4). To obtain the error, an estimate of the *true* integral (to machine epsilon) was calculated using the Matlab function `integral()`. For each formulation of the DRT, the errors were estimated for a single process for three choices of t_0 , and a fixed spreading parameter, $\beta = 0.5$ and $\sigma = \ln(3)$, respectively. The quadrature error for the integration evaluated with respect to s is so small as to be negligible for this problem; the error is always less than 10^{-4} and 10^{-5} , for the RQ and LN cases, respectively, and always far less than the error obtained for quadrature applied to the integration with respect to the variable t . We note further that for any integrand which has similar decay properties on the interval, the same results will apply.

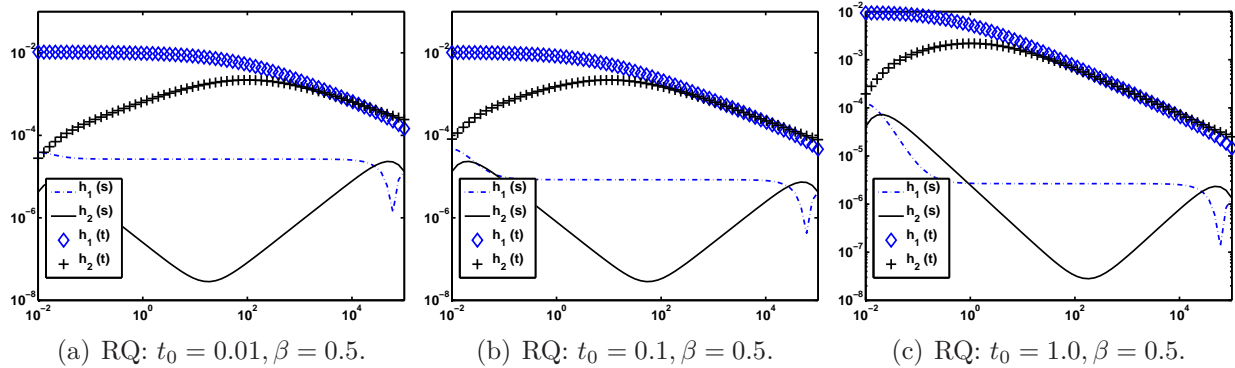


Figure 4: Quadrature error for a single RQ process with $N = 65$ for quadrature in s and t as a function of ω , plotted on a log-log scale, for the kernels corresponding to the real and imaginary components of the impedance.

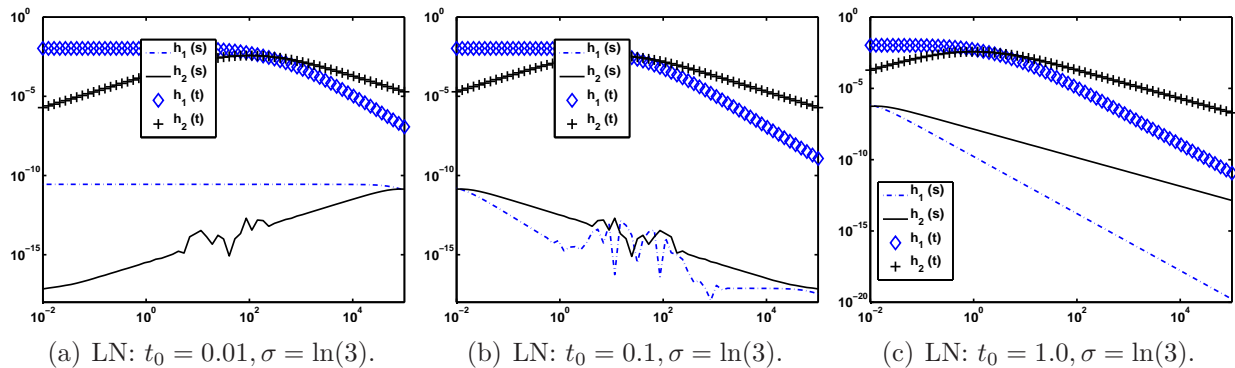


Figure 5: Quadrature error for a single LN process with $N = 65$ for quadrature in s and t as a function of ω , plotted on a log-log scale, for the kernels corresponding to the real and imaginary components of the impedance.

3.2.2. Improved Quadrature

Although we have shown that the error is small, the quadrature (3.5) can be further improved as an approximation to the improper integral in (3.5). It was noted in [19] that the quadrature can be improved for the case of kernel h_2 by extrapolating the data outside the given interval by a straight line. Because the composite trapezium rule is based on linear interpolation on each interval, it is immediately possible to extend the range of the integration by an interval Δs , or indeed on any arbitrary interval, on either side by an extrapolation that assumes $H(s_N + \Delta s) = H(s_1 - \Delta s) = 0$, leading to the modification

$$\int_{-\infty}^{\infty} h(\omega, e^s) f(s) ds \approx \int_{s_1 - \Delta s}^{s_N + \Delta s} h(\omega, e^s) f(s) ds \approx \Delta s \sum_{n=1}^N h(\omega, e^{s_n}) f(s_n). \quad (3.7)$$

Here the only change is that the weight on the first and last terms is no longer halved. This extends the finite range for the quadrature, but does not handle the entire truncation.

Suppose now that $f(s) > 0$ and $\lim_{s \rightarrow \pm\infty} f(s) = 0$, then analytic integration gives

$$\int_{s_N}^{\infty} f(s) h_k(\omega, e^s) ds \leq f(s_N) \int_{s_N}^{\infty} h_k(\omega, e^s) ds = f(s_N) r_{k,N}(\omega, e^{s_N}), \quad (3.8)$$

$$r_{k,N}(\omega, e^{s_N}) := \begin{cases} \frac{1}{2} \ln(1 + (\omega e^{s_N})^{-2}) & k = 1 \\ \frac{\pi}{2} - \tan^{-1}(\omega e^{s_N}) & k = 2, \end{cases} \quad (3.9)$$

while

$$\int_{-\infty}^{s_1} f(s) h_2(\omega, e^s) ds \leq f(s_1) \int_{-\infty}^{s_1} h_2(\omega, e^s) ds = f(s_1) r_{2,1}(\omega, e^{s_1}) \quad (3.10)$$

$$r_{2,1}(\omega, e^{s_1}) := \tan^{-1}(\omega e^{s_1}). \quad (3.11)$$

For the real kernel at the left hand end, separating out the kernel integration in the same way is not useful. Instead we must use again the assumption that $f(s)$ decays fast enough that $f(s_1 - \Delta s) = 0$, (or equivalently that the entire integrand decays fast enough), and set $r_{1,1}(\omega, e^{s_1}) = \frac{1}{2} \Delta s h_1(\omega, e^{s_1})$. Putting these results together leads to the modified quadrature rule which more accurately accounts for the integration outside the range determined by I_s ,

$$\int_{-\infty}^{\infty} h_k(\omega, e^s) f(s) ds \approx \Delta s \sum_{n=1}^N h_k(\omega, e^{s_n}) f(s_n) + f(s_N) r_{k,N}(\omega, e^{s_N}) + f(s_1) r_{k,1}(\omega, e^{s_1}). \quad (3.12)$$

We emphasize the dependence here on the kernel of the integrand in obtaining this result, demonstrating the relative independence of the result on a sufficiently smooth DRT.

3.2.3. Truncation and Quadrature Error

The accuracy of (3.12) as an approximation to the improper integral in (3.5) depends on the quadrature error (3.6) and the truncation error

$$e_k(\omega) = \left| \int_{-\infty}^{s_1} h_k(\omega, s) f(s) ds + \int_{s_N}^{\infty} h_k(\omega, s) f(s) ds - f(s_1) r_{k,1}(\omega, s_1) - f(s_N) r_{k,N}(\omega, s_N) \right|.$$

Let $I_L = [-\infty, s_1]$, and $I_R = [s_N, \infty]$, and assume that I_s has been chosen appropriately for the given data, so that $f(s)$ is monotonically decreasing on both I_L and I_R , i.e. there exists $\epsilon > 0$ such that $|f(s)| \leq \epsilon$, $s \in I_L \cup I_R$. Then considering first $k = 2$

$$\begin{aligned} e_2(\omega) &\leq \left(\max_{s \in I_L} |f(s) - f(s_1)| r_{2,1}(\omega, e^{s_1}) \right) + \left(\max_{s \in I_R} |f(s) - f(s_N)| r_{2,N}(\omega, e^{s_N}) \right) \\ &\leq \epsilon (r_{2,1}(\omega, e^{s_1}) + r_{2,N}(\omega, e^{s_N})) = \epsilon \left(\frac{\pi}{2} + \tan^{-1}(\omega e^{s_1}) - \tan^{-1}(\omega e^{s_N}) \right) \leq \epsilon \pi \end{aligned}$$

providing the total error for kernel h_2

$$E_2(\omega) \leq \epsilon \pi + \frac{(s_N - s_1)^3}{12N^2} |H_2''(\zeta)|. \quad (3.13)$$

For $k = 1$

$$e_1(\omega) \leq \left(\int_{-\infty}^{s_1} h_1(\omega, e^s) f(s) ds - \frac{\Delta s}{2} h_1(\omega, e^{s_1}) f(s_1) \right) + \left(f(s_N) \frac{1}{2} \ln(1 + (\omega e^{s_N})^{-2}) \right).$$

For the first term observe $h_1(\omega, e^s) < 1$ for $s \in I_L$ and that the trapezoidal error bound can be applied. Then, assuming $\int_{-\infty}^{s_1 - \Delta s} f(s) \leq \delta(f)$, and using $\zeta \in [s_1 - \Delta s, s_1]$, we obtain

$$\int_{-\infty}^{s_1} h_1(\omega, e^s) f(s) ds - \frac{\Delta s}{2} h_1(\omega, e^{s_1}) f(s_1) \leq \frac{(\Delta s)^3}{12} |H_1''(\zeta)| + \frac{\Delta s}{2} f(s_1 - \Delta s) + \delta(f),$$

and

$$\begin{aligned} e_1(\omega) &\leq \frac{(\Delta s)^3}{12} |H_1''(\zeta)| + \frac{\Delta s}{2} \epsilon + \delta(f) + \left(\frac{\epsilon}{2} \ln(1 + (\omega e^{s_N})^{-2}) \right) \\ &\leq \frac{\epsilon}{2} (\Delta s + \ln(2)) + \frac{(\Delta s)^3}{12} |H_1''(\zeta)| + \delta(f), \end{aligned}$$

where we use $\omega e^{s_N} = \omega/\omega_1$. Therefore, now with $\zeta \in I_L$

$$E_1(\omega) \leq \frac{\epsilon}{2} (\Delta s + \ln(2)) + \delta(f) + \frac{(s_N - s_1)^3}{12N^3} (N + 1) |H_1''(\zeta)|. \quad (3.14)$$

In contrast to (3.13) this bound depends explicitly on the truncation error $\delta(f)$. On the other hand, for practical N and I_s , $(\Delta s + \ln(2)) < 2\pi$. The two bounds are thus very similar, both depending on the interval I_s , and the smoothness of the integrand.

This analysis which examines the quadrature and truncation error together, contrasts the approach in [27] which found the bounds for each error separately, based explicitly on the use of $g_{LN}(t)$. The same approach can be applied to examine the truncation error for $g_{RQ}(t)$, and is presented in Appendix A. In particular the bound for $\delta(f)$, which explicitly depends on f , is provided by (A.4) for f_{RQ} while the equivalent result for f_{LN} can be found in [27]. We deduce that the total model errors in (3.13)-(3.14) may be assumed small for the standard DRTs which decay quickly away from their centers at t_0 and have sufficiently small second derivatives. Moreover, these bounds improve on those in [27] through the use of the improved quadrature in s to take account of the extended range, thus reducing the size of the error introduced by truncating the improper integral. Further, these results are largely independent of the specific DRT, for any DRT satisfying reasonable decay and smoothness assumptions in s -space.

4. Numerical Algorithms

We now turn to the numerical solution of the ill-posed system of equations defined by (3.12). In the subsequent discussion, matrices created from the original formulation of the problem will be referred to without superscripts, while those created with the change of variable have a superscript s .

4.1. Right Preconditioning

Suppose that the measurements for the impedance are represented by the components of vector \mathbf{b} and that the unknowns $f(s_n)$ are components of the vector \mathbf{x}_1 . Then the matrix equation, $A^s \mathbf{x}_1 \approx \mathbf{b}$, for \mathbf{x}_1 is obtained from (3.5) with $A_{mn}^s = \Delta s'' h(\omega_m, e^{s_n})$, with the double prime indicating the halving for $n = 1$ and $n = N$. With the improved quadrature indicated in (3.12) the components in A_{mn}^s are modified accordingly. In comparison, the discretization for $g(t_n) = f(s_n)/t_n$ is given by $A\mathbf{x} \approx \mathbf{b}$ where \mathbf{x} has components of $g(t)$ and $\text{diag}(\mathbf{t})\mathbf{x} = \mathbf{x}_1$. Contrasting these two formulations we see that the change of variables is effectively a *right* preconditioning of the original system: $A \text{diag}(1./\mathbf{t})\mathbf{x}_1 = \mathbf{b}$. However, $A \text{diag}(1./\mathbf{t}) \neq A^s$. The entries in each column differ in that the weights a_n in (3.4) after division by t_n are proportional to $\sinh(\Delta s)$, excepting scale factors for $n = 1$ and $n = N$, as compared to Δs for matrix A^s . When Δs is small, for large enough N , however, $\Delta s \approx \sinh(\Delta s)$, so that the two matrices are nearly equal [10]. We have already shown that the change of variables impacts the modeling error, we now consider its impact as a right preconditioner on the stability of the underlying system matrices.

4.2. Conditioning

The stability of the solution of a system of linear equations $A\mathbf{x} \approx \mathbf{b}$ is well understood, see e.g. [4, 7, 11]. Given the singular value decomposition (SVD), $A = U\Sigma V^T$, the naive solution is $\mathbf{x} = V\Sigma^{-1}U^T\mathbf{b} = \sum_{i=1}^N (\mathbf{u}_i^T \mathbf{b})/\sigma_i \mathbf{v}_i$, where \mathbf{u}_i and \mathbf{v}_i are the i th columns of U and V , respectively, and σ_i is the i th singular value of A . The sensitivity of this solution to errors (noise) in given measurements \mathbf{b} can be examined via the Picard plot, [13], which illustrates the values of σ_i , $|\mathbf{u}_i^T \mathbf{b}|$, and the ratio $|\mathbf{u}_i^T \mathbf{b}|/\sigma_i$. If σ_i decay faster than $|\mathbf{u}_i^T \mathbf{b}|$, a small perturbation in the true value of \mathbf{b} will be amplified and the solution will be dominated by noise. Figure 6 compares the Picard plots for a given simulation of \mathbf{b} with $N = M = 65$ measurements for kernel h_1 , for both t and s quadrature, matrices A_1 and A_1^s , respectively. For A_1 , $|\mathbf{u}_i^T \mathbf{b}|/\sigma_i$ grow beginning at $i = 1$, while for A_1^s they only begin to grow consistently around $i = 28$.

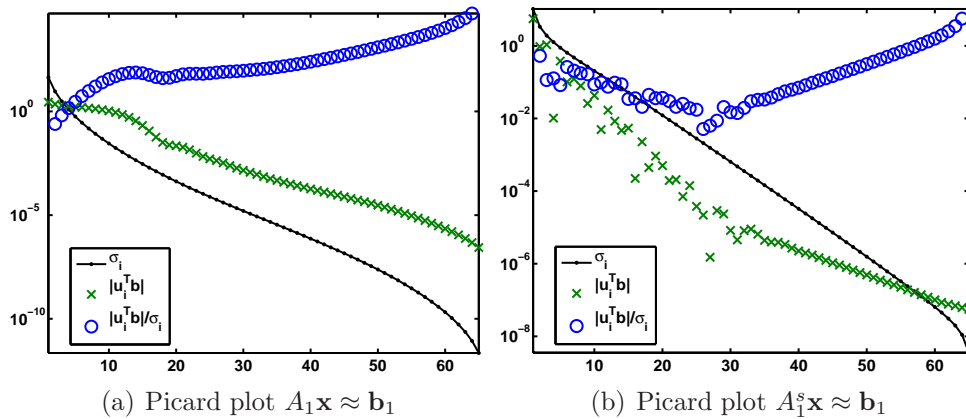


Figure 6: Right hand side \mathbf{b} generated with a single RQ process with $t_0 = 10^{-2}$ and $\beta = 0.8$, using $N = 65$ and ω logarithmically spaced on the interval $[1e - 2, 1e + 5]$.

The sensitivity shown in Figure 6 can be exposed in part by examining the condition number, $\text{cond}(A)$, independent of the measurement \mathbf{b} . A more informative analysis, however,

considers not only the condition but also its impact on the calculation of the basis vectors for the solution formed from the columns of the SVD matrices U and V . It can be shown, e.g. [14], that these columns predominantly approximate single frequency components. This frequency content can be visualized by forming the normalized cumulative periodogram (NCP) for the vector regarded as a discrete time sampling of a continuous function, as explained in the context of examining the residual vector in [12, 29] and the basis vectors in [27]. Vectors which are primarily contaminated by noise have an NCP which falls within Kolmogorov-Smirnov bounds for a chosen confidence level, [6]. Figure 7 contrasts the NCPs of the matrices A_1 and A_1^s , illustrating the better separation of the frequency content for the basis vectors formed from matrices U and V for matrix A_1^s . This suggests greater confidence in the use of a higher number of basis terms in the solution with the right preconditioned matrix. A similar conclusion follows when comparing the matrices for the kernel h_2 .

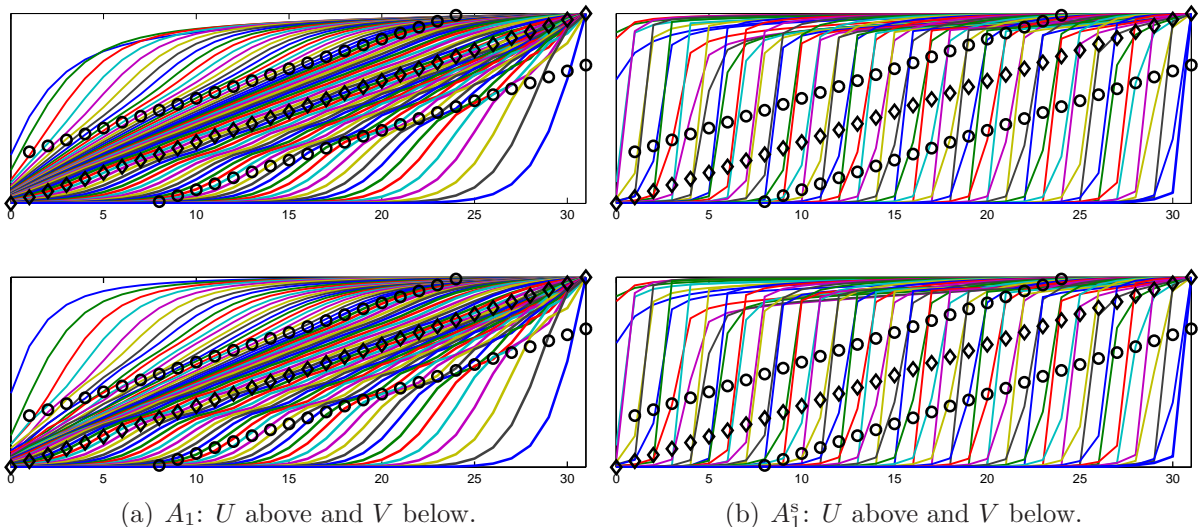


Figure 7: Normalized Cumulative Periodograms and Kolmogorov-Smirnov 95% confidence bounds for white noise for the matrices A_1 and A_1^s . The NCPs for A_2 and A_2^s show a similar separation of the frequency content of the respective basis vectors.

Further demonstration of the impact of the right preconditioning is provided in Table 3 which gives the condition of matrices for the t and s quadrature, for a selection of choices for $I_t = [T_{\min}, T_{\max}]$ with $N = 65$. It is clear that the choice for I_t , and hence I_s , has a large impact on the conditioning of the problem. For instance, if the range for t is too wide, the matrices will have several nearly linearly dependent columns, which greatly increases the condition number of the matrix, and increases the dimension of the numerical null space. Likewise, if the range for t is too narrow, there will be nearly linearly dependent rows, again increasing the condition number of the matrix. When the reciprocal relationship $t = 1/\omega$ is used to pick the sampling in t the optimal condition is obtained in both cases, as shown by the bold face row of the table.

In general there are relatively few measurements of the impedance for the particular biofuel application that can be used to find the solution. Typically there are on the order of $N = 65$ usable values for each of Z_1 and Z_2 , after estimates for the resistances R_{pol} and R_0 in (1.1) have been found. It was shown in [27] that in order to make use of all available

data, it is generally desirable to combine the matrices A_1 and A_2 into the stacked matrix $A_3 = [A_1; A_2]$ of size $2N \times N$, hence using systems associated with both kernels. Further, the overdetermined system can be replaced by a system using a square matrix A_4 of size $2N \times 2N$ through increasing the sampling used in the quadrature for the kernel equations, hence providing increased resolution in the discretization of the solution vector. The same approach can be used for the s -quadrature matrices A_1^s and A_2^s yielding matrices A_3^s and A_4^s . In practice, therefore, it is the impact of the scaling on these augmented matrices which is also significant.

The results in Table 3 are given for the scaled matrices calculated using (3.5). To see that the improvement in the quadrature has little impact on the overall conditioning, the condition numbers of the matrices A_1 to A_4 for various quadrature rules, as noted by the respective equation numbers, are also shown in Table 4. Overall, the right preconditioned matrices, regardless of selection of the system, exhibit better but still not ideal conditioning, so that the problem remains ill-posed and the solution is subject to noise-contamination.

T_{\min}	T_{\max}	A_1	A_2	A_1^s	A_2^s
$1e - 6$	$1e + 1$	$9.70e + 17$	$6.28e + 18$	$2.83e + 17$	$1.90e + 17$
	$1e + 2$	$6.47e + 17$	$1.05e + 20$	$2.99e + 17$	$2.41e + 17$
	$1e + 3$	$4.73e + 18$	$7.45e + 19$	$4.58e + 20$	$6.22e + 18$
$1e - 5$	$1e + 1$	$2.06e + 19$	$1.74e + 18$	$8.17e + 17$	$6.40e + 17$
	$1e + 2$	$1.94e + 13$	$1.78e + 13$	$2.94e + 09$	$7.43e + 07$
	$1e + 3$	$2.20e + 18$	$3.64e + 19$	$2.12e + 20$	$1.87e + 18$
$1e - 4$	$1e + 1$	$5.05e + 21$	$1.55e + 20$	$4.38e + 19$	$2.44e + 18$
	$1e + 2$	$1.52e + 21$	$1.99e + 18$	$1.09e + 20$	$3.90e + 18$
	$1e + 3$	$6.49e + 19$	$6.98e + 18$	$1.30e + 21$	$1.41e + 20$

Table 3: Condition numbers for matrices A_1 , A_2 , A_1^s , and A_2^s for $I_t = [T_{\min}, T_{\max}]$ and ω logarithmically spaced on the interval $[1e - 2, 1e + 5]$.

Quad	Equation	A_1	A_2	A_3	A_4
t	(3.4)	$1.5e + 13$	$1.4e + 13$	$7.5e + 12$	$4.1e + 20$
s	(3.5)	$2.9e + 09$	$7.4e + 07$	$4.6e + 08$	$2.3e + 18$
s	(3.7)	$3.1e + 09$	$7.9e + 07$	$5.0e + 08$	$9.1e + 17$
s	(3.12)	$2.8e + 09$	$7.4e + 07$	$4.6e + 08$	$9.0e + 18$

Table 4: Comparing condition number of matrices with different quadratures for the optimal selection of the nodes for t_n , using $t = 1/\omega$. In this case, as compared to Table 3 the matrices are also reduced to size $N = 64$, consistent with the loss of data when estimating R_0 and R_{pol} in (1.1).

4.3. Regularization

Given the ill-conditioning of the system matrices, regularization is required in order to select an acceptable solution which provides a reasonable fit to the measured data, but is at the same time controlled in its growth with respect to a chosen norm. There is an extensive

literature discussing multiple formulations, e.g. [11, 13, 14, 17, 33] and, for problems of this type, Tikhonov regularization is frequently applied e.g. [19, 27, 35]. The solution is then recast as the solution of the regularized problem

$$\mathbf{x} = \arg \min \{ \|A\mathbf{x} - \mathbf{b}\|^2 + \lambda^2 \|L\mathbf{x}\|^2 \}, \quad (4.1)$$

where λ is a parameter affecting the amount of regularization applied and L is a matrix chosen so the growth of \mathbf{x} is controlled relative to the L -weighted norm. Typical choices for L are approximations to derivative operators of order 0, 1, or 2. For small problems the λ -dependent solution of (4.1) can be expressed in terms of the SVD, ($L = I$), or generalized singular value decomposition (GSVD), for other noninvertible choices for L , e.g. [11].

The choice of the regularization parameter λ is a nontrivial but well-studied problem. There are many algorithms available to choose this parameter. In general, these can be divided into two categories: those which require some knowledge of the characteristics and magnitude of the noise present in the right hand side, and those which do not. Techniques such as the discrepancy principle [11], the unbiased predictive risk estimator (UPRE) [33] and the χ^2 method [25] fall in the first category, while more heuristic methods such as the LC criterion, the quasi-optimality criterion, and generalized cross-validation (GCV) fall in the second, [13]. The NCP criterion applied to the residual for the data fit, which is based on work in [28] and then extended in [12, 29], falls between these two categories. It requires that the noise be white, or can be whitened, but does not require an estimate of its magnitude.

The LC criterion is commonly used when no information on the noise distribution is available. It relies on the fact that when plotted on a logarithmic scale, the weighted norm $\|L\mathbf{x}\|$ and the data fidelity norm $\|A\mathbf{x} - \mathbf{b}\|$ tend to form an L-shaped curve. That is, for a value of λ near the corner, an increase in λ would tend to increase the residual norm without reducing the solution norm much, while a decrease in λ would increase the solution norm without much reducing the residual norm. The SVD and GSVD allow the simple construction of the L-curve, and the corner is generally determined by finding the point of maximum curvature, as implemented in [13].

The NCP approach is based on the assumption that for an appropriately chosen λ the noise in the measurements is transferred to the residual vector so that it is completely dominated by white noise. By calculating the NCP of the residual for suitably selected values of λ , the smallest value which produces a residual vector reasonably approximating white noise may be found. A common statistical test for white noise uses the Kolmogorov-Smirnov statistic to compare the residual NCP with the cumulative distribution function of a uniform distribution. This test is described in more detail in, e.g., [6].

4.4. Non-negative Least-Squares

It was suggested in [24] that the solution of the DRT problem should use the additional information on the DRT, namely that $g(t)$ (and its cousin $f(s)$) are distribution functions satisfying $g(t) \geq 0$ for all t . Augmenting (4.1) by this constraint, yields the NNLS formulation

$$\mathbf{x} = \arg \min \{ \|A\mathbf{x} - \mathbf{b}\|^2 + \lambda^2 \|L\mathbf{x}\|^2, \text{ s.t. } \mathbf{x} \geq 0 \}, \quad (4.2)$$

for which efficient algorithms are available, given a specific choice for λ , including for instance the algorithm in [17], which is implemented in Matlab. On the other hand, because we cannot

immediately express the solution in terms of an expansion, many common parameter choice methods, such as the GCV and UPRE, are less feasible for finding a suitable λ . For this small problem, $N \approx 65$, we explore the use of the two parameter choice methods, the LC criterion and the NCP analysis of the residual vector.

For both LC and NCP, a standard approach for finding the optimal regularization parameter can still be applied. Specifically, solutions of (4.2) can be found for a range of values for λ . Then the LC or NCP, respectively, is applied to assess the quality of each solution, as briefly described for (4.1) in Section 4.3. It is only necessary that an algorithm for the solution of (4.2) is available, e.g. `lsqnonneg` which is the implementation of [17] in Matlab. To verify that our approach is indeed robust to the choice of the algorithm we also consider solutions using the CVX package, [8, 9]. This contrasts with the parameter choice method presented in [24] that relies on a specific implementation of the NNLS algorithm.

5. Simulation Results

The performance of the algorithms discussed and analyzed in Section 3 is investigated for simulated data sets exhibiting properties seen in practical situations. The data sets are described first in Section 5.1. For each data set extensive comparisons have been performed using both matrices A_3 and A_4 , in order to assess whether the better conditioning of A_3 or the better resolution offered by A_4 prevails as the optimum in each case. These examinations have demonstrated that the additional resolution of A_4 outweighs its worse conditioning as compared to A_3 , (see Table 3). While in many cases the results using A_3 are quite comparable, as noise increases systems solved with matrix A_4 often provide better results. Thus in the presented results here we emphasize the comparisons between the LLS and NNLS methods and do not give results for systems with matrix A_3 . Further results substantiating these comments are given in the supplementary materials [10].

5.1. Data sets

The parameters for the simulated data sets are detailed in Table 5. Simulations A and B assume the existence of two underlying physical processes in the data; C assumes three processes. The RQ model uses the parameters t_0 and β , and the LN model uses the parameters $\mu = \ln(t_0)$ and σ . In each case the multiple processes are weighted by the weights α . Note that the choice using $\mu = \ln(t_0)$ for the LN process provides data which are centered at t_0 in the s -space, and as can be seen in Figures 8(b), (g) and (l), are approximately aligned with the RQ model data. The set of figures for each simulation A to C demonstrates the similarity of the chosen RQ and LN data, indicating the difficulty of distinguishing between these models from the impedance data alone, Figures 8(c)-(e), (h)-(j) and (m)-(o). In all plots, other than the Nyquist, the y -data are plotted against x on a logarithmic scale.

Parameters	t_0	β	σ	α
Simulation A	$[10^{-3.5}, 10^{0.5}]$	$[0.8, 0.8]$	$[\ln(2), \ln(2)]$	$[0.5, 0.5]$
Simulation B	$[10^{-1.5}, 10^{-0.5}]$	$[0.7, 0.8]$	$[\ln(2.4), \ln(2)]$	$[0.35, 0.65]$
Simulation C	$[10^{-3}, 1, 10]$	$[0.8, 0.7, 0.7]$	$[\ln(2), \ln(2.1), \ln(2.2)]$	$[0.6, 0.2, 0.2]$

Table 5: Simulation parameters for simulated test data

The two processes in simulation Set A have peaks that are far enough apart that the individuals processes are effectively separated. In such cases distinct peaks are seen in the plot of $Z_2(\omega)$ at ω values which correspond to the reciprocals of the peak values in t . Such information can be used to verify the results of the fitting by examining the locations of the resulting peaks, [10]. Moreover, this is therefore a relatively well-behaved situation for which it should be possible to separate the underlying processes from measured data. In contrast, the two processes in set B are close but the existence of two peaks is not clear from Z_2 . For the three processes in set C the first is distinct in time from the latter two, which are close and overlapping for larger time. Again the impedance data does not clearly indicate the number of processes in the data.

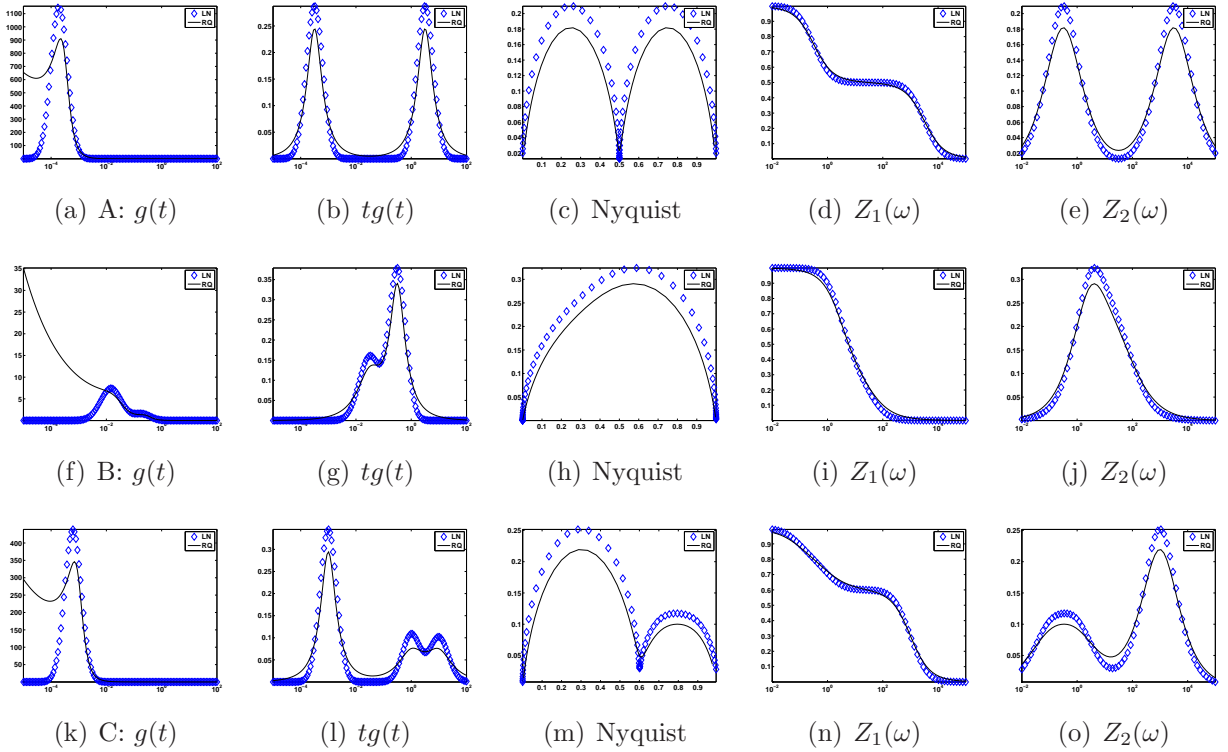


Figure 8: Visualization of the simulation sets in Table 5, simulations A to C in subfigures (a)-(e), (f)-(j) and (k)-(m), respectively. In each plot the RQ simulation is illustrated with the solid line and the LN simulation with the \diamond . Except for the Nyquist plot, the scale of the x -axis is logarithmic.

For testing the algorithms noise was added to the simulated values for Z following (2.1) as discussed in Section 2 for the examination of the NLS fitting. In all cases the data are sampled at 65 points logarithmically spaced on $[\omega_{\min}, \omega_{\max}] = [10^{-2}, 10^5]$, consistent with practical data, and with sampling of the DRT at $t = 1/\omega$ yielding the equal spacing in s -space at 130 points for matrix A_4 . For the results presented here, the noise level $\eta = 10^{-3}$ corresponding to .1% noise was chosen. Further results in [10] use noise levels 1% and 5%. While the higher noise levels, particularly around 1% may be more consistent with practical data, the actual noise level for the measured data is unknown. On the other hand, even with the lower noise level the benefit of using the NNLS will become clear in Sections 5.2-5.3.

5.2. Parameter Choice Methods

The NCP or residual periodogram (RP) was presented in [12, 28, 29] as a parameter choice method for the Tikhonov LLS problem (4.1). The use of the NCP applied to the residual for finding the optimal parameter for the NNLS problem in (4.2) is, however, to the best of our knowledge novel. We therefore first contrast the use of the LC and NCP for parameter choice in the context of the NNLS constrained problem, with the three standard choices of zero ($L = I$), first ($L = L_1$) and second order ($L = L_2$) derivative operators. These can be obtained using the function `get_1` in the Regularization toolbox [13]. The LC is also implemented in the Regularization toolbox, while for the NCP we use the modification of the `nep` in the toolbox, as used also for examining the frequency content of the basis vectors as shown in Section 4.3. For both the NCP and L-Curve methods, solutions were found for 50 choices of λ logarithmically spaced between $10^{-3.5}$ and $10^{1.5}$. The optimal λ for the LC was chosen using the corner of the LC, while for the NCP method, the Kolmogorov-Smirnov confidence level for white noise uses $p = 0.2$. Each simulation was tested over 50 realizations of .1% white noise.

For each noise realization the following information was recorded: the optimal solution obtained by the NCP and LC parameter choice methods, with the optimally found λ_{NCP} and λ_{LC} , and the optimal solution over all 50 choices for λ , with the respective λ_{opt} , as measured with respect to the absolute error in the s -space. The geometric means of λ_{NCP} and λ_{LC} were calculated over all 50 noise realizations. The absolute error for each choice of λ was also recorded for each noise realization, and the mean of these absolute errors taken to give an average error for a given λ which can be visualized against λ . This follows the analysis presented in [24] for the examination of the optimal regularization parameter. In the plots we thus show the average error against λ indicated by the \circ plot. On the same plot we indicate by the vertical lines the minimum λ_{opt} , and the geometric means for λ_{NCP} and λ_{LC} , as the solid (red), dashed (green) and dot-dashed \circ (blue) vertical lines, respectively. For each simulation set the same procedure was performed for all smoothing norms L . To demonstrate the dependence of the obtained solution on the optimal parameter, an example representative noise realization was chosen in each case and the solutions found using the chosen optimal parameters were compared with the exact solution. These are indicated by the solid line (black), \diamond (red), \times (green) and \circ (blue), for the exact, λ_{opt} , λ_{NCP} , and λ_{LC} solutions, respectively.

The results are illustrated in Figures 9-14. Figures (a)-(c) in each case indicate the mean error results for the different smoothing norms, and (d)-(f) demonstrate the sensitivity, or lack thereof, of the solution to the choice of λ near the optimum. We see that the results are remarkably consistent; the results with the identity weighted norm are generally less robust, while overall the NCP parameter choice marginally outperforms the LC. On the other hand, we also conclude that the use of either parameter choice method is robust in terms of representing the *optimal* but practically *unknown* solution. Thus the NCP is to be preferred for finding a suitable regularization parameter, and the L_1 operator provides a compromise between over smoothing (a reduced peak) by L_2 and under smoothing by $L = I$. Additional results for higher noise levels are provided in [10]. There it is shown that for noise levels at 5% the results deteriorate significantly in terms of the ability to accurately determine the number of processes, that the LC results are significantly under smoothed and that the extra resolution of matrix A_4 is most obviously worthwhile, a result that is not at

all clear by examination of the relative error. Overall, it is also clear that the LN processes are better resolved than those given by the RQ. This is not surprising given the graph of the RQ DRT for small t , see e.g. Figure 1(a), 3(a).

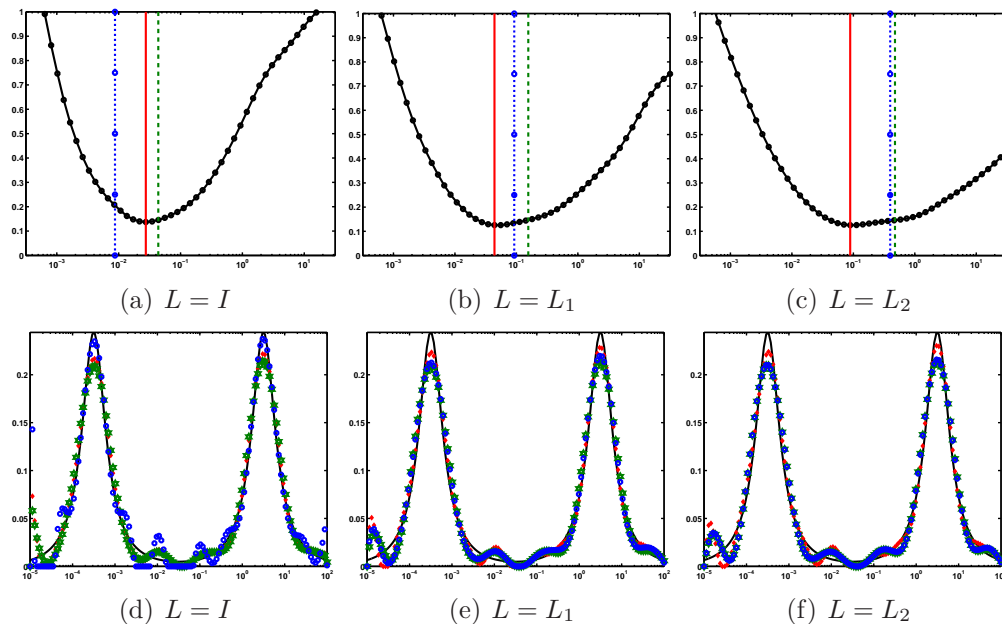


Figure 9: Mean error and example `1sqnonneg` NNLS solutions. .1% noise, RQ-A data set, matrix A_4 .

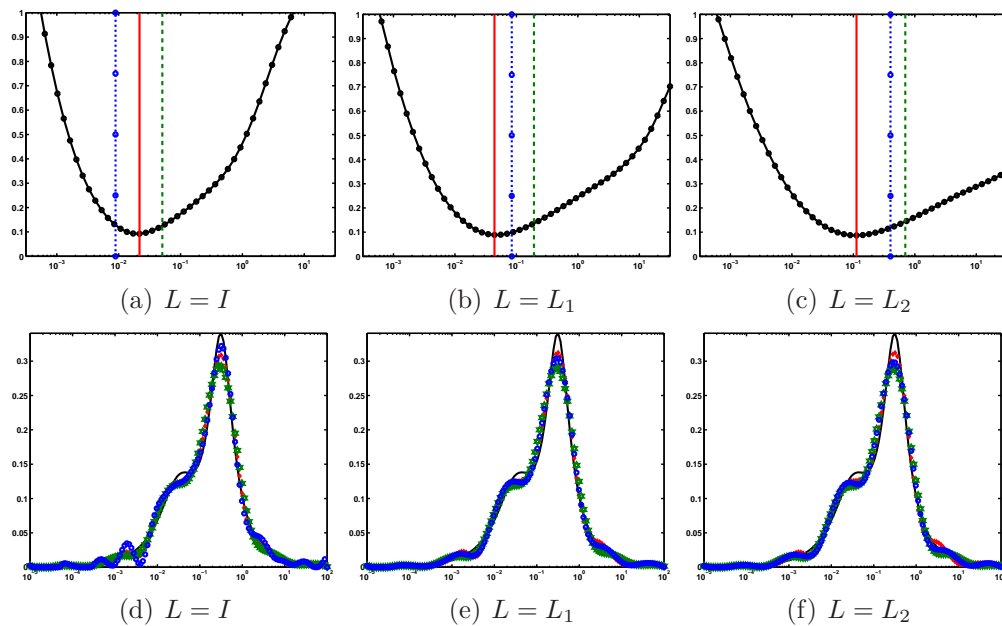


Figure 10: Mean error and example `1sqnonneg` NNLS solutions. .1% noise, RQ-B data set, matrix A_4 .

To verify that these conclusions are not just a feature of the particular choice of the NNLS solver, we also repeated the experiments replacing the `1sqnonneg` solver for (4.2).

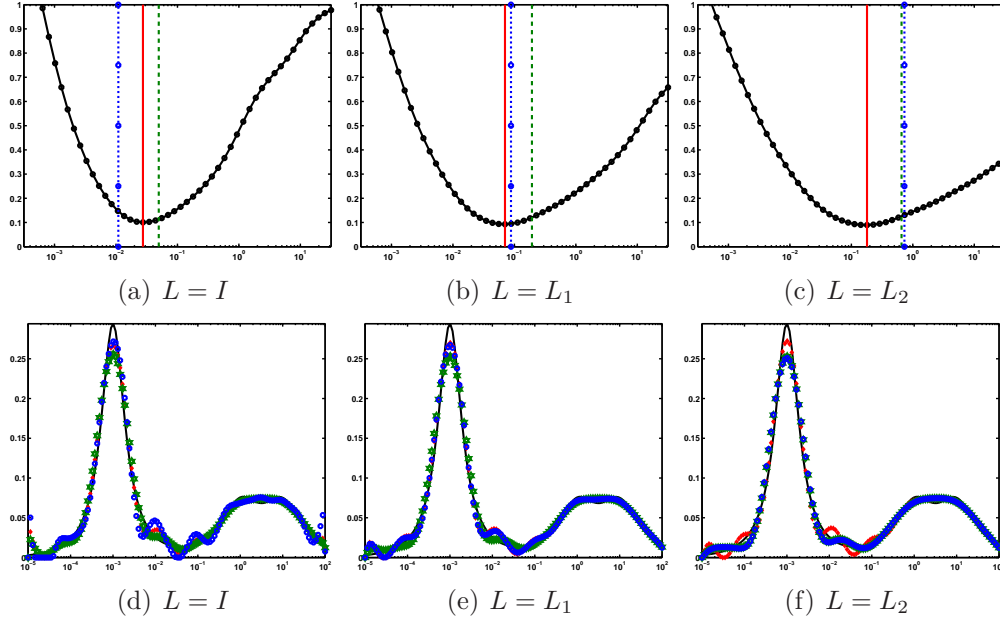


Figure 11: Mean error and example `lsqnonneg` NNLS solutions. .1% noise, RQ-C data set, matrix A_4 .

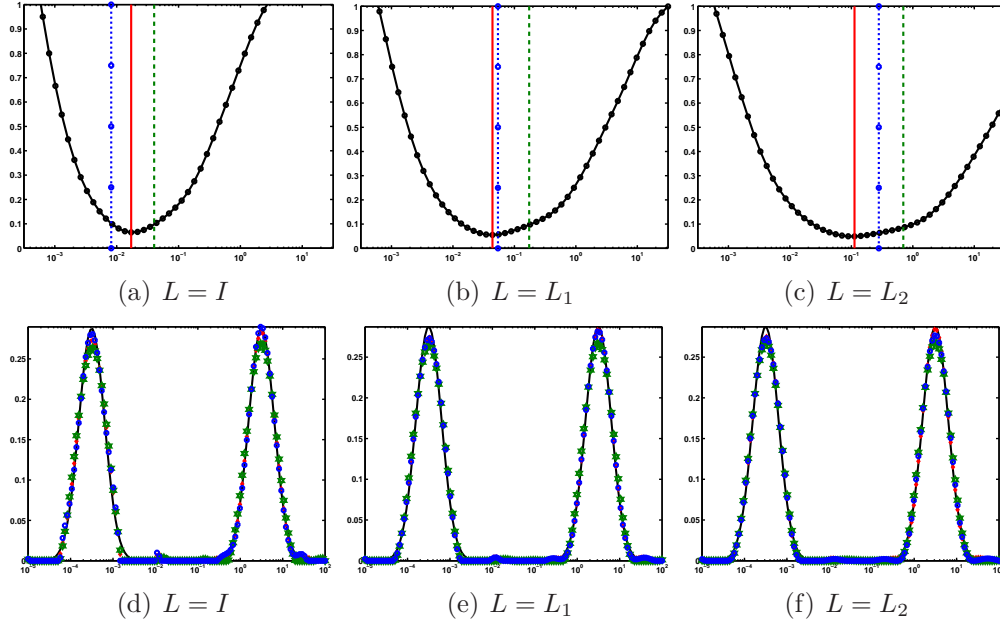


Figure 12: Mean error and example `lsqnonneg` NNLS solutions. .1% noise, LN-A data set, matrix A_4 .

Several algorithms for NNLS are provided in the literature, see e.g. [3, 8, 15, 31], but not all are relevant for dense but small ill-posed problems,. We chose CVX, which is easily implemented in Matlab, and is well-known as a robust package for specifying and solving convex programs, [8, 9]. These results are presented in Figures 15-20 for exactly the same set of data. The results are remarkably consistent and demonstrate that the suggested technique to find the optimal regularization parameter for Tikhonov regularized non-negative least squares is robust to the underlying algorithm. Additional experiments, not reported here,

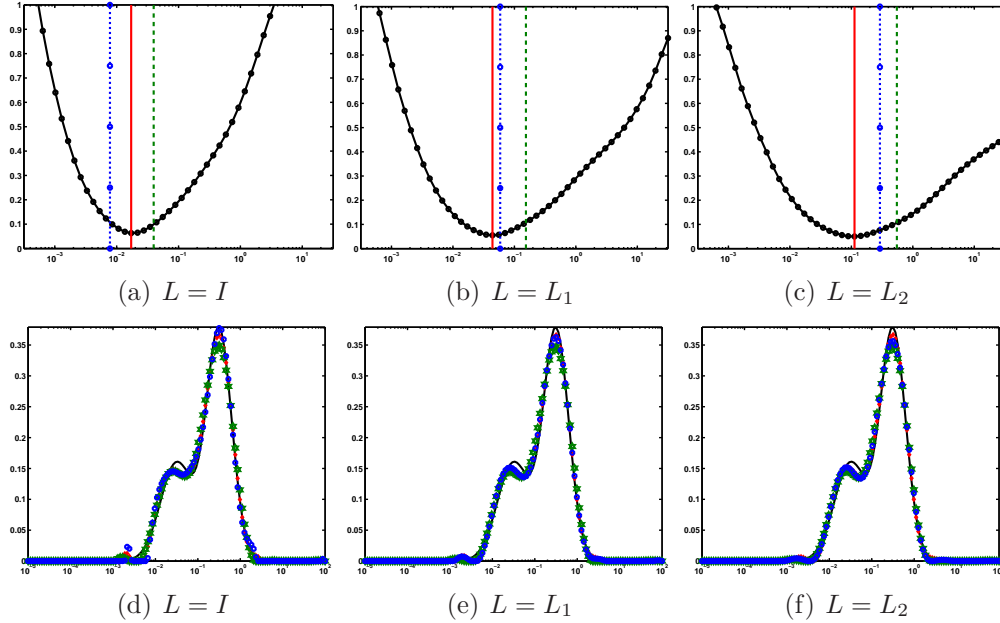


Figure 13: Mean error and example `lsqnonneg` NNLS solutions. .1% noise, LN-B data set, matrix A_4 .

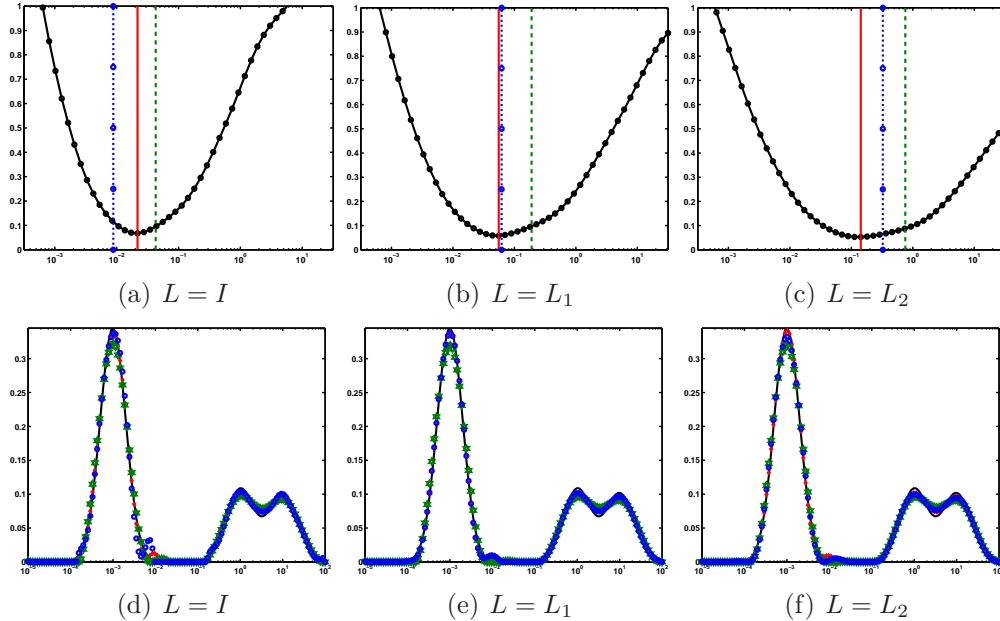


Figure 14: Mean error and example `lsqnonneg` NNLS solutions. .1% noise, LN-C data set, matrix A_4 .

also used the subspace Barzilai and Borwein (SBB) algorithm, presented in [15, 16]. We found that this algorithm was overall less robust for solving the small-scale non-negative least squares problems described here, which does not contradict the results in [15]. Still, where the algorithm succeeded, for larger choices of λ , again NCP and L-curve estimates of the optimal choice for λ are feasible. A selection of these results is presented in the supplementary materials, as are further experiments for higher noise levels using both CVX

and `lsqnonneg`, [10].

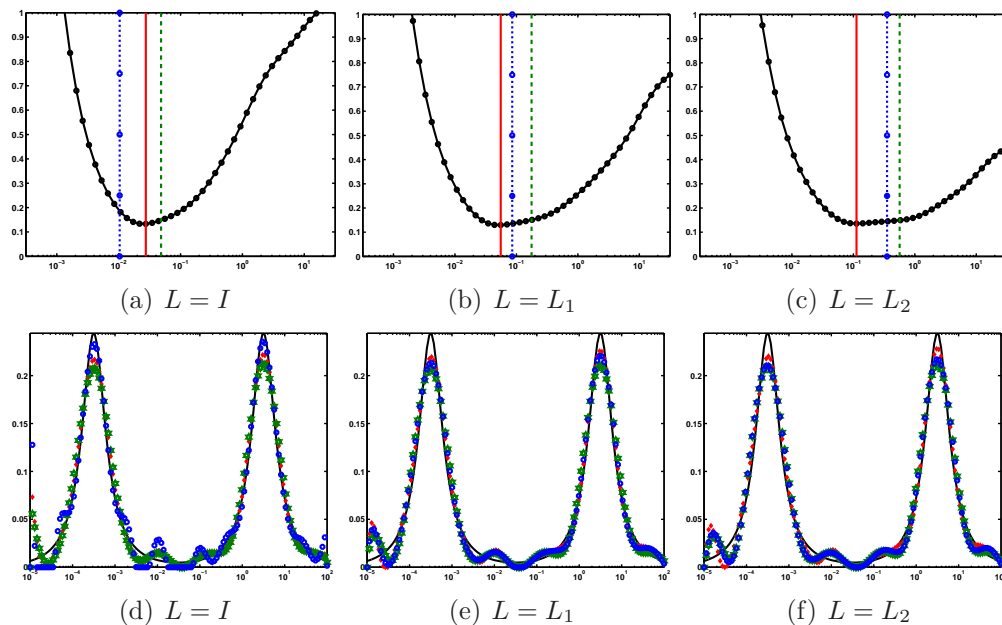


Figure 15: Mean error and example CVX NNLS solutions. .1% noise, RQ-A data set, matrix A_4 .

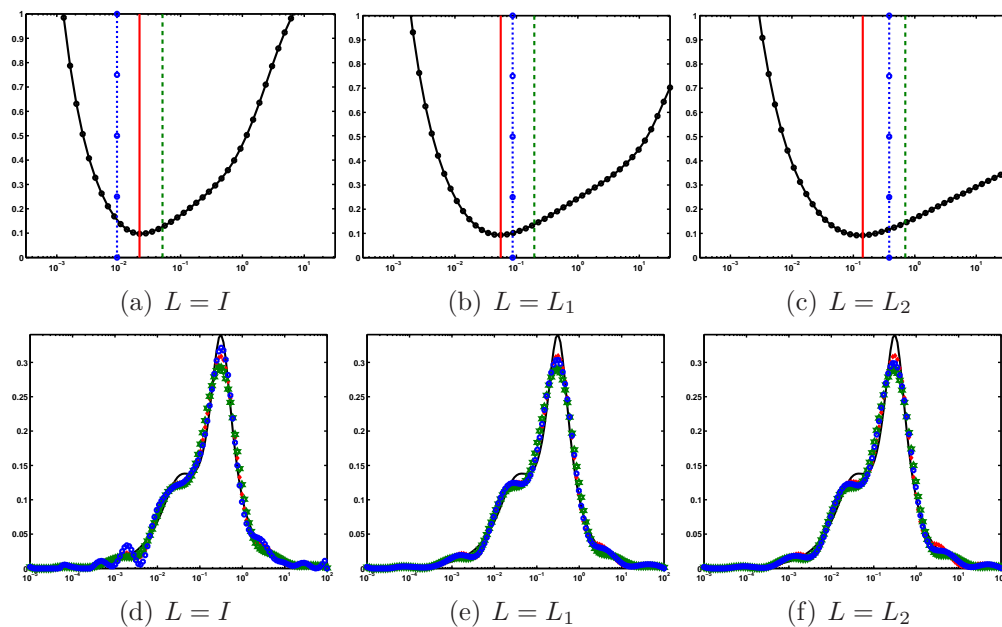


Figure 16: Mean error and example CVX NNLS solutions. .1% noise, RQ-B data set, matrix A_4 .

5.3. Comparison of LLS and NNLS

Finally we present a comparison of the NNLS results with those that are obtained using the Tikhonov regularization (4.1) for the same two parameter choice methods in order to

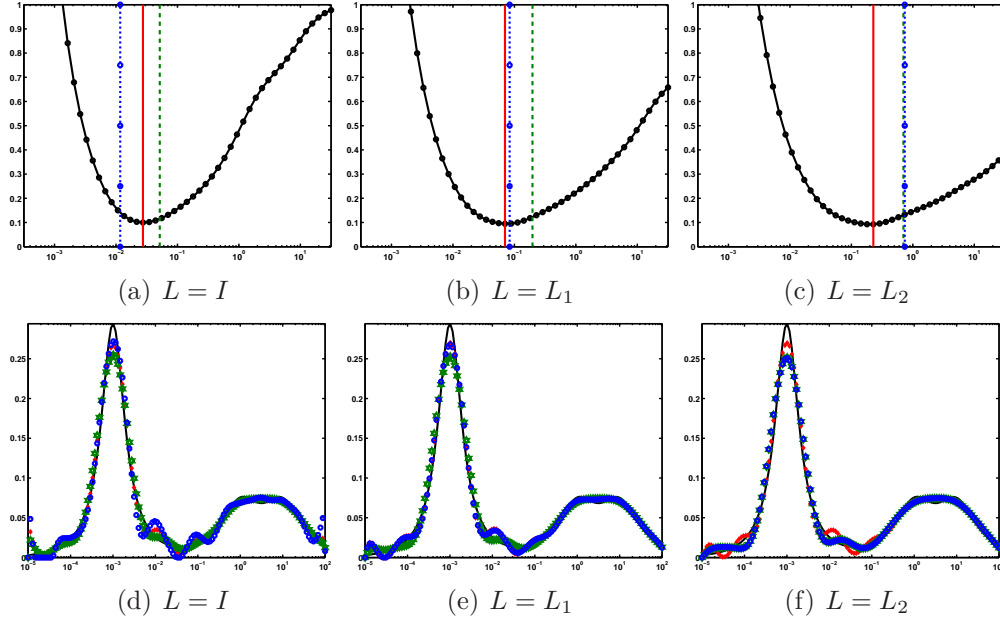


Figure 17: Mean error and example CVX NNLS solutions. .1% noise, RQ-C data set, matrix A_4 .

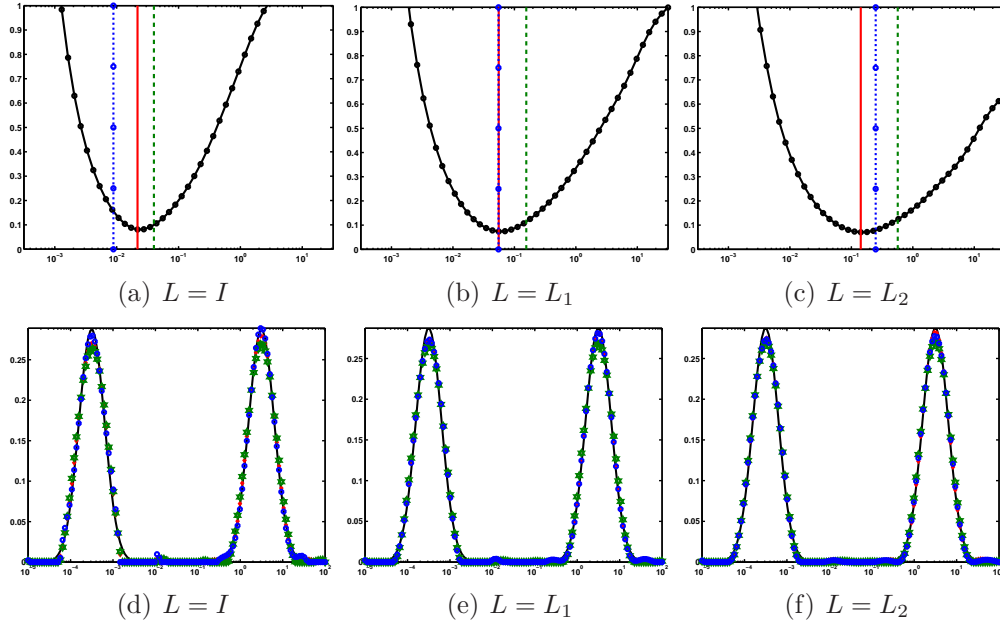


Figure 18: Mean error and example CVX NNLS solutions. .1% noise, LN-A data set, matrix A_4 .

assess whether the extra cost of the NN constraint is necessary. While extensive results were given in [27] for (4.1), these were only for the t -quadrature matrices. The results for the A_3 matrix and other noise levels are given in [10], where comparative tables of relative errors are also given. Here we present the results visually in Figures 21-26 equivalent to the NNLS results in Section 5.2. We see again that we cannot always anticipate for the optimum choice of λ chosen by a specific algorithm will provide a solution with the minimum error, as measured by sampling over multiple choices for the regularization parameter. On the other

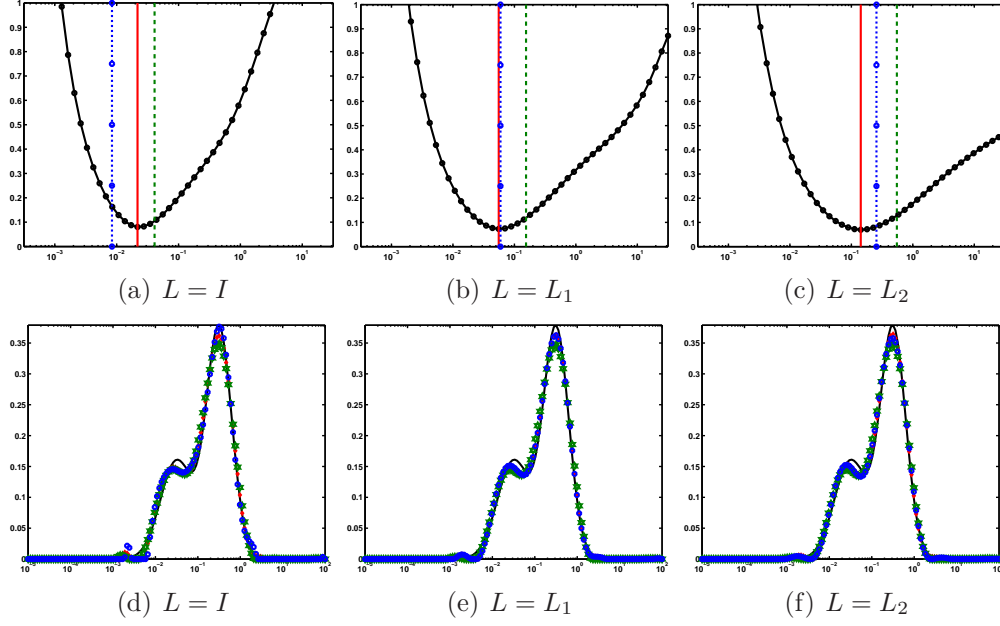


Figure 19: Mean error and example CVX NNLS solutions. .1% noise, LN-B data set, matrix A_4 .

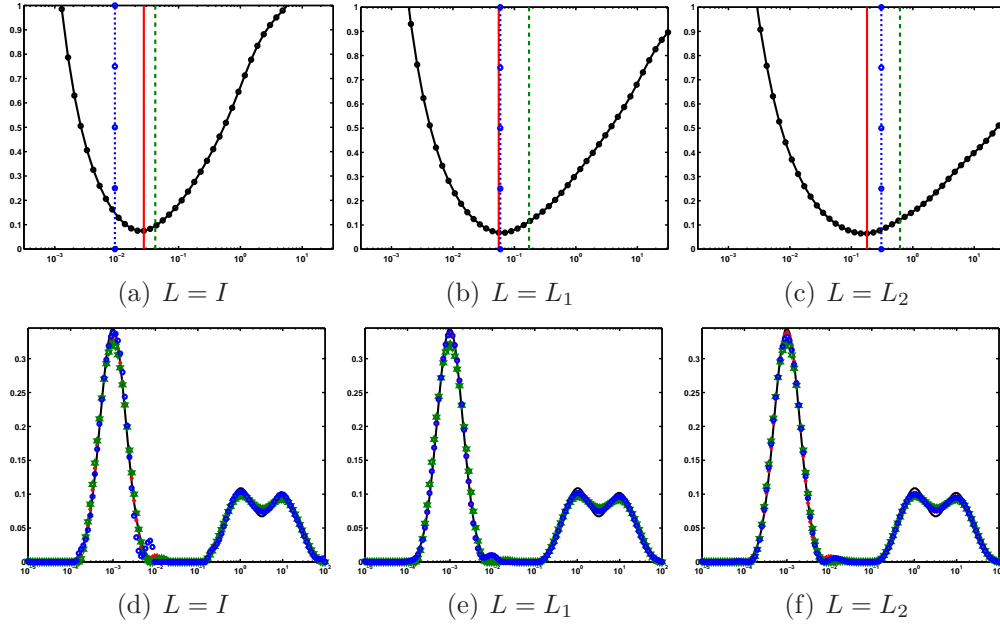


Figure 20: Mean error and example CVX NNLS solutions. .1% noise, LN-C data set, matrix A_4 .

hand, the performance of these two parameter choice methods for the LS problem is good evidence that the performance for the NNLS problem is consistent. For the solutions it is evident that NNLS provides better control of oscillations around zero due to the positivity constraint. Moreover, because the NNLS does not need to control these oscillations, solutions are less smooth and provide better resolution of the peaks. Given the sample sizes for the particular microbial fuel cell application, and possibly other electrochemical applications

with limited sampling, the extra minimal cost associated with finding NNLS solutions offers significantly improved results. Indeed for higher noise levels, the LLS solutions offer little reliable information about the actual physical processes of the model.

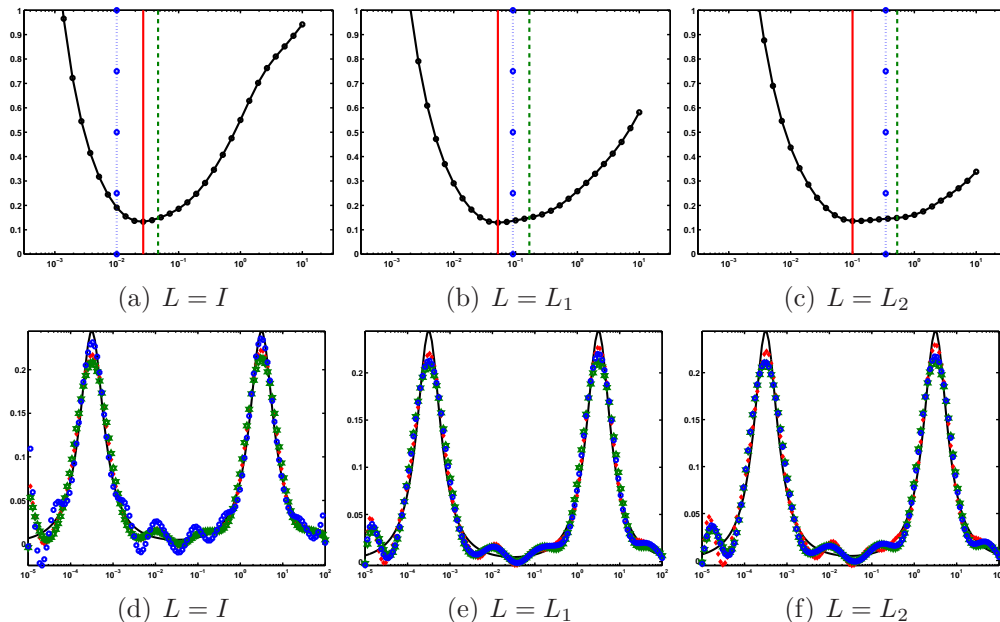


Figure 21: Mean error and example LLS solutions. .1% noise, RQ-A data set, matrix A_4 .

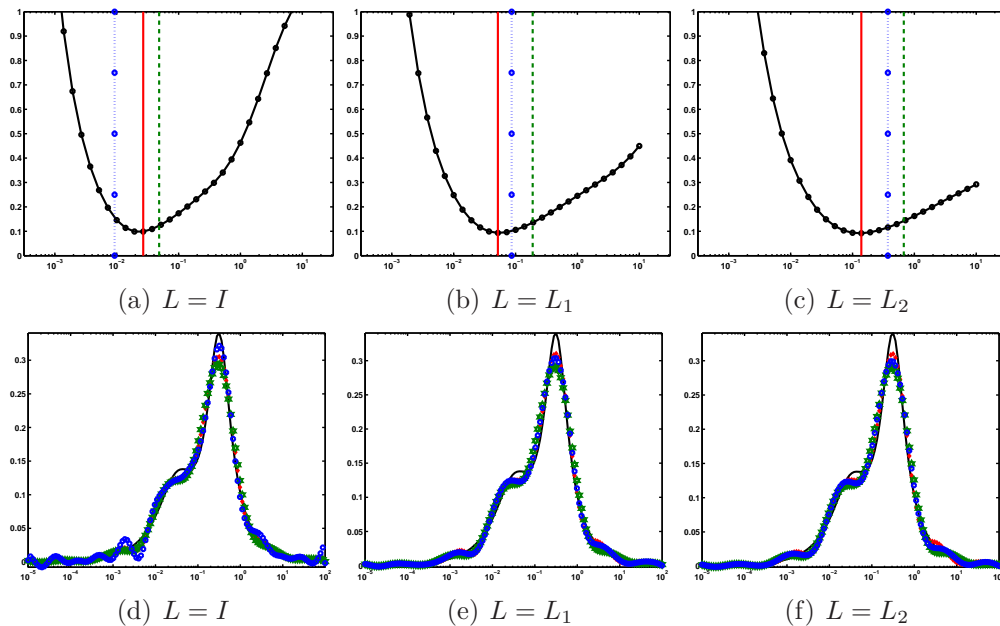


Figure 22: Mean error and example LLS solutions. .1% noise, RQ-B data set, matrix A_4 .

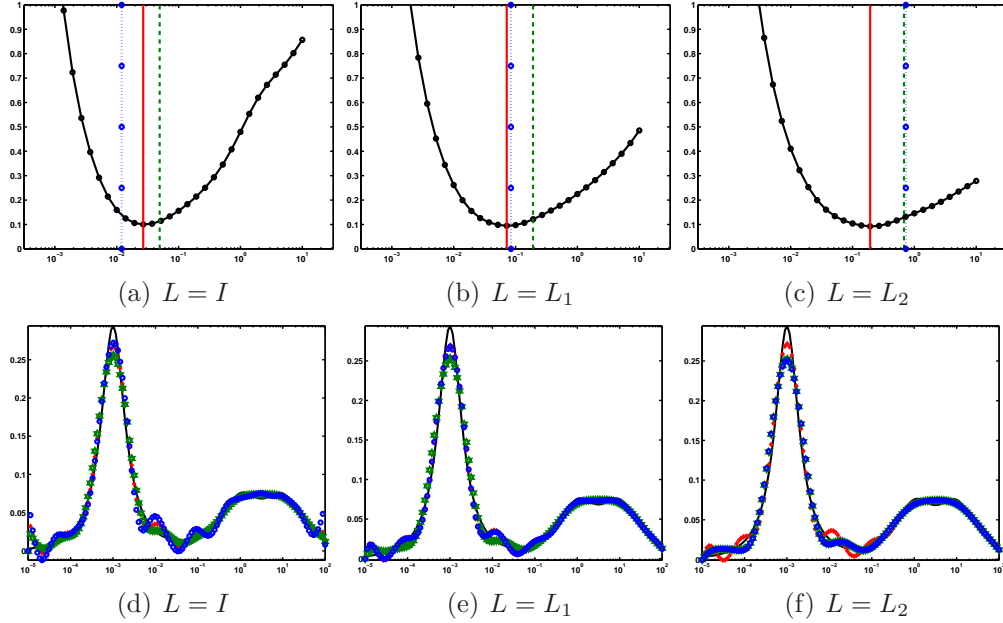


Figure 23: Mean error and example LLS solutions. .1% noise, RQ-C data set, matrix A_4 .

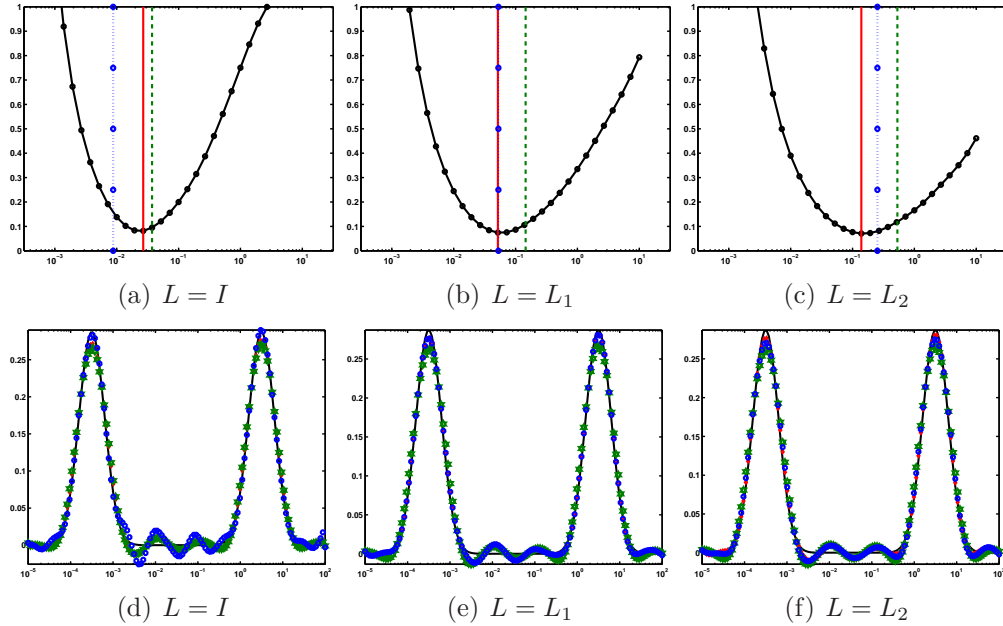


Figure 24: Mean error and example LLS solutions. .1% noise, LN-A data set, matrix A_4 .

6. Conclusion

The inverse problem associated with impedance spectroscopy of fuel cells has been discussed. Two models for the underlying distribution function of relaxation times have been considered. If the model for the DRT is known to be log-normal or RQ, then nonlinear fitting of the data using the right model can be done very consistently, while trying to fit to the wrong model consistently returns inaccurate results. Moreover, when the noise level is

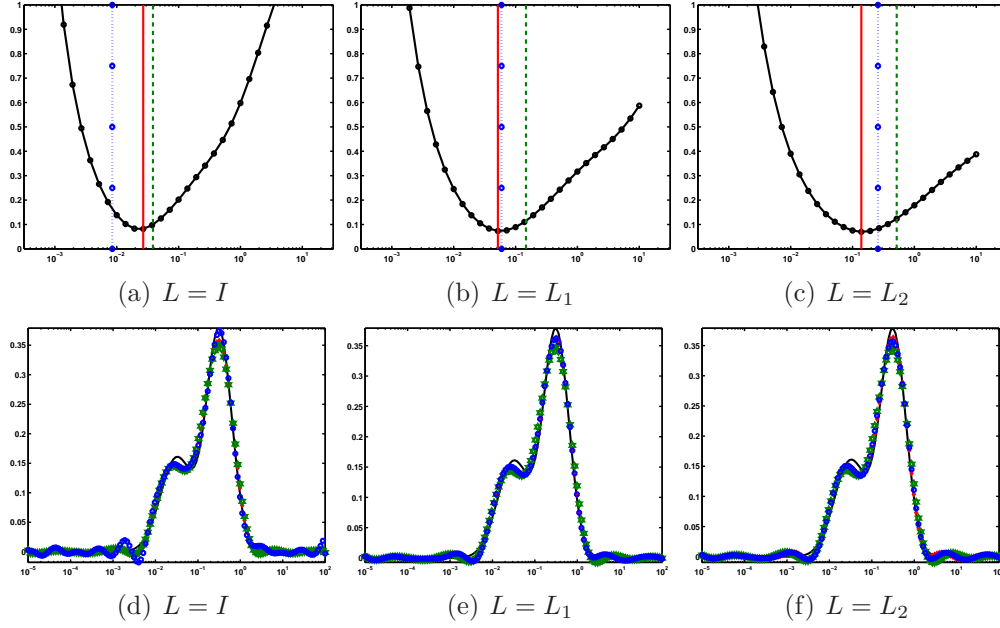


Figure 25: Mean error and example LLS solutions. .1% noise, LN-B data set, matrix A_4 .

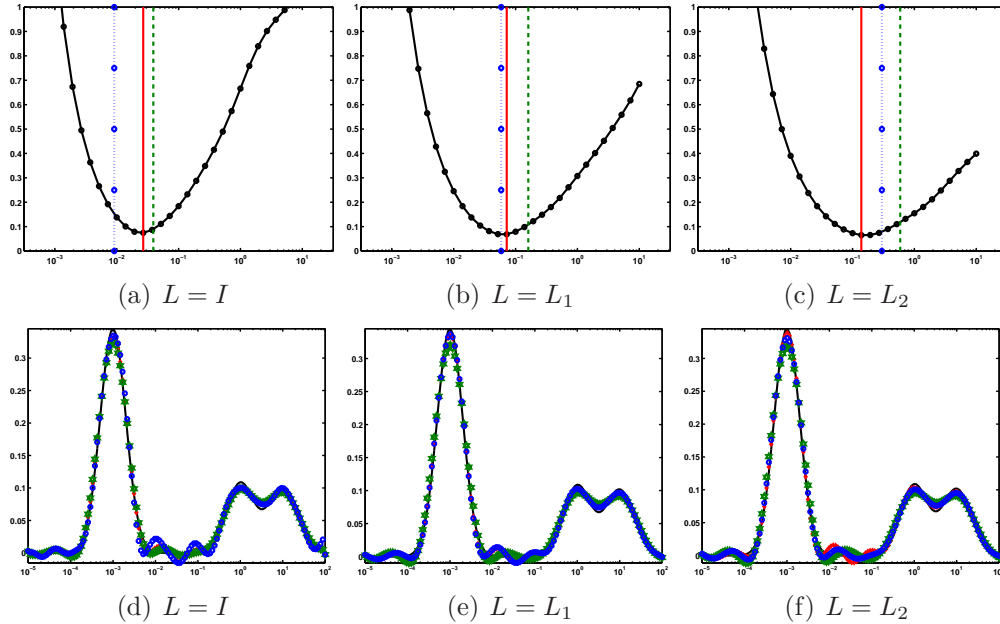


Figure 26: Mean error and example LLS solutions. .1% noise, LN-C data set, matrix A_4 .

high, distinguishing which model to use in NLS fitting becomes problematic and may yield results that do not accurately describe the data. If the physical model for the process is not known, the inverse problem for estimating the DRT needs to be solved by finding a solution to the discrete linear system. For this system, it has been shown that the model error can be made negligible by a change of variables and by extending the effective range of quadrature. Moreover, the conditioning of the problem improves considerably when the

right-preconditioned matrices A^s are used.

To obtain feasible solutions to the discrete linear systems additional constraints are required. Simulations with artificial, but realistic, data demonstrate that the use of NNLS with a smoothing norm provides higher quality solutions than those obtained without the NN constraint. Using higher-order smoothing norms also reduces the error in the solutions. Moreover, the LC and NCP criteria are effective regularization parameter choice techniques in the context of the NNLS formulation. Indeed, the use of the NCP criterion for parameter choice with the NN constraint is a novel development of more general use for NNLS in other applications, and has been validated for use both with `lsqnonneg` in Matlab and the CVX software, [8, 9].

Although these results have been verified within the context of the analysis of fuel cells, there is no reason to suppose that they would not be relevant within the broader framework of solving Fredholm integral equations for other applications. In particular, an approach for optimal regularization parameter estimation in the context of non-negatively constrained Tikhonov least squares has been provided.

7. Acknowledgements

We would like to thank an anonymous referee who suggested applying the non-negative constrained Tikhonov regularization with algorithms other than `lsqnonneg`, hence leading to stronger conclusions on the relevance of our techniques. Authors Hansen, Hogue and Sander were supported by NSF CSUMS grant DMS 0703587: “CSUMS: Undergraduate Research Experiences for Computational Math Sciences Majors at ASU”. Renault was supported by NSF MCTP grant DMS 1148771: “MCTP: Mathematics Mentoring Partnership Between Arizona State University and the Maricopa County Community College District”, NSF grant DMS 121655: “Novel Numerical Approximation Techniques for Non-Standard Sampling Regimes”, and AFOSR grant 025717 “Development and Analysis of Non-Classical Numerical Approximation Methods”. Popat was supported by ONR grant N000141210344: “Characterizing electron transport resistances from anode-respiring bacteria using electrochemical techniques”. All authors wish to thank Professor César Torres from Arizona State University for discussions concerning the EIS modeling.

Appendix A. Truncation error

In (3.4)-(3.5) the semi-infinite (infinite) integrals are necessarily truncated. An analysis of the impact of the truncation for the lognormal DRT was presented in [27]. Here we investigate the extension of this result for the RQ model. Consider the single RQ process given by (3.2). The error from the upper truncation of the integral of this distribution at s_N is given by

$$E_{\text{trunc}}^u(s_N) = \int_{s_N}^{\infty} f(s) ds = \frac{1}{2} - \frac{\tan^{-1} \left(\tan \left(\frac{\pi\beta}{2} \right) \tanh \left(\frac{\beta(s_N - \ln(t_0))}{2} \right) \right)}{\pi\beta}. \quad (\text{A.1})$$

Thus, in order to have $E_{\text{trunc}}^u(s_N) < \delta$, we must have

$$s_N > \frac{2}{\beta} \tanh^{-1} \left(\frac{\tan \left(\frac{\pi\beta}{2} (1 - 2\delta) \right)}{\tan \frac{\pi\beta}{2}} \right) + \ln(t_0). \quad (\text{A.2})$$

Similarly, because the error from the lower truncation is given by

$$E_{\text{trunc}}^1(s_1) = \int_{-\infty}^{s_1} f(s) ds = \frac{1}{2} + \frac{\tan^{-1} \left(\tan \left(\frac{\pi\beta}{2} \right) \tanh \left(\frac{\beta(s_1 - \ln(t_0))}{2} \right) \right)}{\pi\beta}, \quad (\text{A.3})$$

keeping $E_{\text{trunc}}^1 < \delta$ requires

$$s_1 < -\frac{2}{\beta} \tanh^{-1} \left(\frac{\tan \left(\frac{\pi\beta}{2} (1 - 2\delta) \right)}{\tan \frac{\pi\beta}{2}} \right) + \ln(t_0). \quad (\text{A.4})$$

Note that these error bounds are symmetric for $t_0 = 1$; then $s_1 = -s_N$, $E_{\text{trunc}}^1(s_1) = E_{\text{trunc}}^u(s_N)$. On the other hand, as t_0 moves to the right or left of 1, the bounds for s_N , s_1 shift in tandem, and thus we obtain a requirement on the total range

$$E_{\text{trunc}} = E_{\text{trunc}}^u + E_{\text{trunc}}^1 < 2\delta \text{ for } s_N - s_1 > \frac{4}{\beta} \tanh^{-1} \left(\frac{\tan \left(\frac{\pi\beta}{2} (1 - 2\delta) \right)}{\tan \frac{\pi\beta}{2}} \right). \quad (\text{A.5})$$

Once E_{trunc} is bounded, Lemma 1 from [27] can be applied directly, without proof.

Lemma 1. *Suppose that s_1 and s_N are such that the upper and lower truncation errors are each less than δ , i.e.,*

$$E_{\text{trunc}}^u(s_N) = \int_{-\infty}^{\infty} f(s) ds - \int_{-\infty}^{s_N} f(s) ds < \delta \text{ and } E_{\text{trunc}}^1(s_1) = \int_{-\infty}^{\infty} f(s) ds - \int_{s_1}^{\infty} f(s) ds < \delta.$$

Then

$$\begin{aligned} E_{\text{trunc}}^1(\omega) &= \int_{-\infty}^{\infty} \frac{f(s)}{1 + \omega^2 e^{2s}} ds - \int_{s_1}^{s_N} \frac{f(s)}{1 + \omega^2 e^{2s}} ds \leq \delta \left(1 + \frac{1}{1 + \omega^2 e^{2s_N}} \right) \leq 2\delta \\ E_{\text{trunc}}^2(\omega) &= \int_{-\infty}^{\infty} \frac{\omega e^{2s} f(s)}{1 + \omega^2 e^{2s}} ds - \int_{s_1}^{s_N} \frac{\omega e^{2s} f(s)}{1 + \omega^2 e^{2s}} ds \leq (E_2)_{\min} + (E_2)_{\max} < \delta, \end{aligned}$$

where

$$\begin{aligned} (E_2)_{\min} &= \int_{-\infty}^{s_1} \frac{\omega e^s f(s)}{1 + \omega^2 e^{2s}} ds \leq \begin{cases} \delta \frac{\omega e^{s_1}}{1 + \omega^2 e^{2s_1}} \leq \frac{\delta}{2} & \omega e^{s_1} < 1 \\ \frac{\delta}{2} & \omega e^{s_1} \geq 1 \end{cases} \\ (E_2)_{\max} &= \int_{s_N}^{\infty} \frac{\omega e^s f(s)}{1 + \omega^2 e^{2s}} ds \leq \begin{cases} \delta \frac{\omega e^{s_N}}{1 + \omega^2 e^{2s_N}} \leq \frac{\delta}{2} & \omega e^{s_N} \geq 1 \\ \frac{\delta}{2} & \omega e^{s_N} < 1. \end{cases} \end{aligned}$$

Observe here that for the standard choice $s_1 = \ln(T_{\min})$ and $s_N = \ln(T_{\max})$, with $T_{\min} = 1/\omega_{\max}$ and $T_{\max} = 1/\omega_{\min}$, then $\omega e^{s_1} < 1$, $\omega e^{s_N} > 1$, and the bounds for E_2 simplify as given. Provided that the range for the integration moves with the location of t_0 , either to the right or left, (A.5), the error is controlled appropriately. If on the other hand we always assume $t_0 = 1$ and pick the range symmetrically with respect to 0, the error will depend on the actual location of t_0 .

References

- [1] K.E. Atkinson, *An Introduction to Numerical Analysis*, (2nd ed.), New York: John Wiley & Sons, 1998, ISBN 978-0-471-50023-0.
- [2] E. Barsukov, J.R. Macdonald, editors, *Impedance Spectroscopy: Theory, Experiment, and Applications*, John Wiley and Sons, Hoboken, New Jersey, United States, 2005.
- [3] S Bellavia, M Macconi, B Morini *An interior point Newton-like method for non-negative least-squares problems with degenerate solution* Numerical Linear Algebra with Applications, **13**, 10, (2016), 825-846.
- [4] A. Björck, *Numerical Methods for Least Squares Problems*, Soc. for Ind. and Appl. Math., Philadelphia, PA, 1986.
- [5] C. Endler, A. Leonide, A. Weber, F. Tietz, E. Ivers-Tiffée, *Time-dependent electrode performance changes in intermediate temperature solid oxide fuel cells*, J. of the Electrochem. Soc., **157**, (2010), B292-B298.
- [6] W.A. Fuller, *Introduction to Statistical Time Series*, Wiley series in probability and statistics, second edition, Wiley Publications, New York, United States, 1996.
- [7] G. Golub, C. van Loan, *Matrix Computations*, Third Edition, John Hopkins University Press, Baltimore, Maryland, 1996,
- [8] M. Grant, S. Boyd, *CVX: Matlab Software for Disciplined Convex Programming, version 2.1*, <http://cvxr.com/cvx>, (2014)
- [9] M. Grant, S. Boyd, *Graph implementations for nonsmooth convex programs*, in Recent Advances in Learning and Control, Lecture Notes in Control and Information Sciences, Editors: V. Blondel, S. Boyd, H. Kimura, Springer-Verlag Limited, (2008), 95-110, http://stanford.edu/~boyd/graph_dcp.html
- [10] J. Hansen, J. Hogue, G. Sander, R.A. Renaut, *Non-negatively constrained least squares and parameter choice by the residual periodogram for the inversion of electrochemical impedance spectroscopy: Supplementary Materials*, <http://math.la.asu.edu/~rosie/cv0806/node1.html>, 2013.
- [11] P.C. Hansen, *Rank-deficient and discrete ill-posed problems: numerical aspects of linear inversion*, SIAM Series on Fundamentals of Alg, Soc. for Ind. and Appl. Math., Philadelphia, PA, 1998.
- [12] P.C. Hansen, M. Kilmer, R.H. Kjeldsen, *Exploiting residual information in the parameter choice for discrete ill-posed problems*, BIT **46**, (2006), 4159.
- [13] P.C. Hansen, *Regularization Tools Version 4.0 for Matlab 7.3*, Numer. Alg, **46**, (2007), 189-194.
- [14] P.C. Hansen, *Discrete inverse problems: Insight and algorithms*, SIAM Series on Fundamentals of Alg , **7**, Soc. for Ind. and Appl. Math., Philadelphia, PA, 2010.

- [15] D. Kim, S. Sra, and I. S. Dhillon *A Non-monotonic Method for Large-scale Non-negative Least Squares*, Optimization Methods and Software, **28**, 5 (2013), 1012-1039.
- [16] Dongmin Kim, University of Texas, Source code for the Barzilai-Borwein Algorithm, SBB, (2008), <http://www.cs.utexas.edu/~dmkim/Source/software/sbb/sbb.html>.
- [17] C.L. Lawson, R.J. Hansen, *Solving Least Squares Problems*, SIAM Classics in Appl. Math., Soc. for Ind. and Appl. Math., Philadelphia, PA, 1995.
- [18] A. Leonide, *SOFC Modelling and Parameter Identification by means of Impedance Spectroscopy*. KIT Scientific Publishing, 2010.
- [19] A. Leonide, V. Sonn, A. Weber, E. Ivers-Tiffée, *Evaluation and Modeling of the Cell Resistance in Anode-Supported Solid Oxide Fuel Cells*, J. of the Electrochem. Soc. **155**, (1), (2008), B36-B41.
- [20] A. Leonide, B. Ruger, A. Weber, W.A. Meulenber, E. Ivers-Tiffée, *Impedance study of alternative (La,Sr)FeO(3-delta) and (La,Sr)(Co,Fe)O(3-delta) MIEC cathode compositions*, J. of the Electrochem. Soc., **57**, (2010), B234-B239.
- [21] B. Liu, H. Muroyama, T. Matsui, K. Tomida, T. Kabata, K. Eguchi, *Analysis of impedance spectra for segmented-in-series tubular solid oxide fuel cells*, J. of the Electrochem. Soc., **157**, (2010), B1858-B1864.
- [22] B. Liu, H. Muroyama, T. Matsui, K. Tomida, T. Kabata, K. Eguchi, *Gas Transport impedance in segmented-in-series tubular solid oxide fuel cell*, J. of the Electrochem. Soc., **157**, (2011), B215-B224.
- [23] J.R. Macdonald, *Exact and approximate nonlinear least-squares inversion of dielectric relaxation spectra*, J. of Chem. Phys., **102**, 15, (1995), 102:15.
- [24] J. Macutkevicius, J. Banys, A. Matulis, *Determination of the Distribution of the Relaxation Times from Dielectric Spectra*, Nonlinear Anal.: Modelling and Control, **9**, (1), (2004), 7588.
- [25] J. Mead, R.A. Renaut, *A Newton root-finding algorithm for estimating the regularization parameter for solving ill-conditioned least squares problems*, Inverse Problems, (2009), 25(2).
- [26] T. M. Nahir, E.F. Bowden, *The distribution of standard rate constants for electron transfer between thiol-modified gold electrodes and adsorbed cytochrome c*. J. of Electroanal. Chem., **410**, 1, (1996), 9–13.
- [27] R.A. Renaut, R. Baker, M. Horst, C. Johnson D. Nasir, *Stability and error analysis of the polarization estimation inverse problem for microbial fuel cells*, Inverse Probl., **29**, (2013), 045006 (24pp), doi:10.1088/0266-5611/29/4/045006.
- [28] B.W. Rust, *Truncating the singular value decomposition for ill-posed problems*, Technical Report NISTIR 6131., National Institute of Standards and Technology, (1998), URL = <http://math.nist.gov/BRust/pubs/TruncSVD/MS-TruncSVD.ps>.

- [29] B.W. Rust, D.P. O’Leary, *Residual periodograms for choosing regularization parameters for ill-posed problems*, Inverse Probl., **24**, 3, 2008, 034005 - 034035.
- [30] H. Schichlein, A.C. Muller, M. Voigts, A. Krugel, E. Ivers-Tiffée, *Deconvolution of electrochemical impedance spectra for the identification of electrode reaction mechanisms in solid oxide fuel cells*, J. of Appl. Electrochem., **32**, (2002), 875-882.
- [31] M. Slawski, M. Hein, *Non-negative least squares for high-dimensional linear models: consistency and sparse recovery without regularization*, Electronic Journal of Statistics, **7**, 0, (2013), 3004-3056.
- [32] V. Sonn, A. Leonide, E. Ivers-Tiffée, *Combined Deconvolution and CNLS Fitting Approach Appl. on the Impedance Response of Technical Ni/8YSZ Cermet Electrodes*, J. of the Electrochem. Soc., **155**, (7) (2008), B675-B679.
- [33] C.R. Vogel, *Computational Methods for Inverse Problems*, SIAM: Philadelphia, PA, 2002.
- [34] L.C. Ward, T. Essex, B.H. Cornish, *Determination of Cole parameters in multiple frequency bioelectrical impedance analysis using only the measurement of impedances*, Physiol. Meas., **27**, 9, (2006), 839-850.
- [35] J. Weese, *A reliable and fast method for the solution of Fredholm integral equations of the first kind based on Tikhonov regularization*, Comput. Phys. Commun., **69**, (1992), 99-111.